5. Impacts on Ecosystems in East Asia

5.1 Introduction

Forest ecosystems deliver a wide range of essential ecological services, including the provision of natural resources, groundwater recharge, carbon sequestration, and disaster prevention. However, prolonged atmospheric deposition of acidifying substances and associated chemical compounds has the potential to disrupt ecosystem functions and reduce the resilience of forest environments. In many EANET participating countries, emissions of major air pollutants have begun to decline. Nevertheless, experiences from Europe and North America indicate that the recovery of forest ecosystems from acidification has not progressed as expected, and ecological impacts have persisted even after substantial reductions in SO_2 and NOx emissions. Long-term monitoring is essential for understanding the long-term impacts on ecosystems and the process by which they recover.

The EANET has been monitoring key ecosystem components, such as forest vegetation, soil, and inland water, using the standardized methods outlined in Section 5.2 ever since regular-phase monitoring activities began in 2000, in order to assess the impacts of atmospheric deposition on ecosystems. Over more than two decades, substantial datasets have been accumulated across numerous monitoring sites, although data availability and characteristics vary by monitoring item. In addition, since 2010, EANET has promoted catchment-scale analyses that consider biogeochemical cycles in forest ecosystems, enabling qualitative and quantitative examinations of the interrelationships among atmospheric deposition, soil, forest vegetation, and inland water (primarily stream water) within catchment areas. Sections 5.3, 5.4, and 5.5 summarize the characteristics and long-term trends of soil, forest vegetation, and inland water based on datasets available up to 2024 and discuss their relationships with atmospheric deposition using data from the nearest monitoring sites. Furthermore, the results from regular catchment monitoring sites and catchment-scale analyses conducted at other EANET sites up to 2024 are presented in Section 5.6.

5.2 Monitoring methodology

The above monitoring activities have been implemented in accordance with technical documents developed and adopted by the Scientific Advisory Committee of EANET. Specifically, the following technical manuals and guideline have been used:

- *Technical Manual for Soil and Vegetation Monitoring in East Asia* (EANET, 2000)
- *Technical Manual for Inland Aquatic Environment Monitoring in East Asia–2010* (EANET, 2010a)
- *Guideline for Catchment-scale Monitoring in East Asia* (EANET, 2010b)

Monitoring items and recommended frequencies for detecting impacts on ecosystems are summarized in Table 5.2.1. In forest vegetation monitoring, surveys of tree decline, descriptions of trees (tree growth), and understory vegetation surveys are conducted to detect direct impacts of air pollution as well as indirect impacts of acidic atmospheric deposition. In soil monitoring, chemical properties of soils are analyzed to detect soil acidification resulting from atmospheric deposition. In inland aquatic environment monitoring, the properties of lake water or river water are measured to detect inland water acidification. In catchment-scale monitoring, inputs from atmospheric deposition, outputs via stream water, and their balance are evaluated by considering biogeochemical processes within a forest catchment or watershed as a unit area.

Table 5.2.1 Monitoring items and recommended frequencies for detecting impacts on ecosystems

Monitoring	Mandatory items	Recommended frequency
Soil	Chemical properties of soil: pH, Ex-base cations (Ca, Mg, K, and Na), Ex-acidity, Ex-H and Al, and $CaCO_3$ (for calcareous soil only)	Every 3-5 years
Forest vegetation	Surveys of tree decline Description of trees (tree growth) Understory vegetation surveys (species composition)	Once every year Every 3-5 years Every 3-5 years
Inland aquatic environment (inland water)	Properties of lake water or river water: water temperature, pH, EC, alkalinity (Gran's plot titration/pH4.8-endpoint), major cations (NH_4^+, Ca^{2+}, Mg^{2+}, K^+, and Na^+), major anions (SO_4^{2-}, NO_3^-, and Cl^-), other anions (NO_2^- and PO_4^{3-}), water color, DOC/TOC, total P, and total N For lake water only: transparency, DO, chlorophyll a, sediment (SO_4^{2-}, NO_3^-, and NH_4^+ in pore water) For river water only: SS	4 times a year (for lake water) Every one month or two months (for river water) Every 3-5 years (for sediment)
Catchment-scale	Input (total atmospheric deposition): precipitation amount, wet deposition, (dry deposition) and total deposition Output (discharge from a stream): water discharge, stream water chemistry, and chemical discharge Items for biogeochemical processes: soil chemical properties, Plant growth	Continuously (for precipitation), daily, weekly, biweekly, or monthly Continuously (for water discharge), weekly or biweekly, or monthly Utilization of the results of soil monitoring and forest vegetation monitoring

Note: Ex, exchangeable; Ex-H and Al were originally defined as optional items but have been measured at many sites as quasi-mandatory items; EC, electric conductivity; DOC, dissolved organic carbon; TOC, total organic carbon; DO, dissolved oxygen; SS, suspended solids

5.3 Soil chemical properties

Soil monitoring has been conducted at 33 sites in 10 countries, including a pre-survey carried out in 1999. Since 2000, official survey records have been collected in accordance with the *Technical Documents for Soil and Vegetation Monitoring in East Asia* (EANET, 2000). The metadata for each site and the number of surveys conducted are shown in Tables 5.3.1, and 5.3.2, respectively. Over the past 25 years, up to six surveys have been conducted at the most intensively monitored sites, whereas some sites have had no soil monitoring record since 2000 (Table 5.3.2). As shown in the previous chapters, the atmospheric environment has improved over the past decade; therefore, attention should be paid to whether these changes are reflected in soil chemical properties. This section mainly focuses on soil chemical properties pH(H_2O), pH(KCl), exchangeable cations (Ca^{2+}, Mg^{2+}, K^+, Na^+, Al^{3+}, and H^+). First, the distribution of statistics for the entire monitoring period at each site, as well as the factors contributing to this distribution, are presented. Second, changes in soil pH(H_2O) over the 25-year period in relation to atmospheric conditions are discussed.

5.3.1 Distribution of soil chemical properties at EANET sites

As shown in Table 5.3.1, the geographical locations of EANET soil monitoring sites cover a very wide range, extending from high-latitude regions in the Northern Hemisphere to low-latitude equatorial regions. Latitude is directly related to climatic conditions and reflects variations in precipitation and air temperature. These climatic conditions also regulate vegetation and soil formation, which together determine soil type.

Table 5.3.1 Metadata for soil monitoring sites.

Country	Site name	Site code	Corresponding atmospheric monitoring site	Geographical coordinates		MAP[*1]	Forest type [*2]	Soil type
				N Latitude	E Longitude	(mm y^{-1})		WRB [*3]
China	Jinyunshan	CNS004	Jinyunshan	29° 49'	106° 22'	1,207	Evergreen-coniferous	Not specified
	Dabagou	CNS007	Jiwozi	33° 50'	108° 48'	538	Evergreen-coniferous	Not specified
	Xiaoping	CNS009	Xiaoping	24° 51'	118° 2'	1,751	Evergreen-broad-leaved	Not specified
	Zhuxiandong	CNS011	Zhuxiandong	22° 12'	113° 31'	1,729	Evergreen-broad-leaved	Not specified
Indonesia	Bogor Research Forest	IDS002	Serpong	-6° 45'	106° 34'	1,902	Evergreen-broad-leaved	Not specified
Japan	Sekido-san	JPS005	Happo	36° 58'	136° 58'	2,554	Deciduous-broad-leaved	Cambisols
	Horyu-zan	JPS105	Happo	37° 26'	137° 10'	2,554	Deciduous-broad-leaved	Acrisols
	Ijira	JPS006	Ijira	35° 34'	136° 42'	2,900	Evergreen-coniferous	Cambisols
	Yamato	JPS106	Ijira	35° 51'	136° 58'	2,900	Evergreen-coniferous	Andosols
Malaysia	Pasoh 1	MYS001	Petaling Jaya	2° 59'	102° 19'	3,380	Evergreen-broad-leaved	Acrisols
	Pasoh 2	MYS101	Petaling Jaya	2° 59'	102° 19'	3,380	Evergreen-broad-leaved	Acrisols
	Pasoh TEAM Plot 1	MYS201	Petaling Jaya	2° 59'	102° 18'	3,380	Evergreen-broad-leaved	Acrisols
	Pasoh TEAM Plot 8	MYS202	Petaling Jaya	2° 58'	102° 21'	3,380	Evergreen-broad-leaved	Acrisols
	UPMKB 1991	MYS005	—	3° 13'	113° 6'	—	Not specified	Not specified
	UPMKB 2008	MYS105	—	3° 13'	113° 6'	—	Not specified	Not specified
Mongolia	Bogdkhan Mountain	MNS001	Ulaanbaatar	47° 54'	106° 49'	162	Deciduous-coniferous	Not specified
	Terelj Mountain	MNS002	Terelj	47° 59'	107° 29'	164	Not specified	Not specified
Philippines	Mt. Makiling	PHS002	Los Baños	14° 10'	121° 11'	2,043	Evergreen-broad-leaved	Cambisols
	Up Quezon Land Grant	PHS102	Los Baños	14° 10'	121° 11'	2,043	Evergreen-broad-leaved	Nitisols
	La Mesa Watershed	PHS001	Metro Manila	14° 38'	121° 4'	2,881	Evergreen-broad-leaved	Not specified
	Boneco LTER Site	PHS003	Mt. Sto. Tomas	16° 25'	120° 36'	4,243	Evergreen-coniferous	Not specified
R. of Korea	Mt. Naejang	KRS003	Imsil	35° 36'	127° 11'	1,160	Evergreen-coniferous	Not specified
Russia	Irkutsk	RUS003	Irkutsk	52° 14'	104° 15'	424	Evergreen-coniferous	Luvisols
	Bolshie Koty	RUS002	Listvyanka	51° 51'	104° 54'	379	Evergreen-coniferous	Leptosols
	Pereemnaya river catchment	RUS102	Listvyanka	51° 56'	105° 17'	379	Evergreen-coniferous	Leptosols
	Ilchir Lake [*4]	RUS001	Mondy	51° 40'	101° 0'	239	Not specified	Gleysols
	Okinskoe Lake [*4]	RUS101	Mondy	51° 40'	101° 0'	239	Not specified	Podsols
	Solar Observatory	RUS201	Mondy	51° 40'	101° 0'	239	Deciduous-coniferous	Gleysols
	Primorskaya	RUS004	Primorskaya	—	—	768	Deciduous-broad-leaved	Cambisols
Thailand	Vajiralongkorn Dam	THS004	Khanchanaburi	14° 46'	98° 35'	1,563	Evergreen-broad-leaved	Acrisols
	Vajiralongkorn Puye	THS104	Khanchanaburi	14° 46'	98° 35'	1,563	Evergreen-broad-leaved	Luvisols
Vietnam	Cave of Heaven [*4]	VNS002	Hoa Binh	20° 49'	105° 20'	1,800	Not specified	Not specified
	Thang Ranh [*4]	VNS102	Hoa Binh	20° 49'	105° 20'	1,800	Not specified	Not specified

*1, MAP is mean annual precipitation calculated from EANET wet deposition monitoring data.

*2, Forest type was decided from the dominant tree species reported in tree decline monitoring.

*3, Soil type is besed on soil classification of World Reference Base for Soil Resources (IUSS Working Group WRB, 2015).

*4, Grayed rows indicate sites having no official data since 2000.

Table 5.3.2 Monitoring frequency and summary of chemical properties at each site from 2000 to 2024.

Country	Site code	Number of surveys	pH(H_2O)	pH(KCl)	Exchangeable cations ($cmol_c\ kg^{-1}$)					
					Ca^{2+}	Mg^{2+}	K^{+}	Na^{+}	Al^{3+}	H^{+}
China	CNS004	7	4.1 ± 0.2	3.5 ± 0.2	0.32 ± 0.25	0.08 ± 0.05	0.08 ± 0.03	0.02 ± 0.02	5.76 ± 1.60	0.94 ± 0.48
	CNS007	7	6.0 ± 0.4	5.0 ± 0.4	5.05 ± 1.86	0.61 ± 0.36	0.54 ± 0.23	0.17 ± 0.11	0.24 ± 0.24	0.57 ± 0.54
	CNS009	5	4.6 ± 0.2	4.0 ± 0.1	0.03 ± 0.03	0.06 ± 0.02	0.21 ± 0.08	0.09 ± 0.06	4.17 ± 1.48	0.50 ± 0.45
	CNS011	7	4.4 ± 0.3	3.8 ± 0.2	0.94 ± 1.09	0.33 ± 0.36	0.33 ± 0.46	0.22 ± 0.23	1.53 ± 1.04	1.71 ± 1.35
Indonesia	IDS002	5	4.2 ± 0.1	3.7 ± 0.1	1.05 ± 0.44	0.59 ± 0.67	0.09 ± 0.04	0.05 ± 0.06	4.09 ± 0.75	0.56 ± 0.31
Japan	JPS005	5	4.5 ± 0.2	3.7 ± 0.2	0.40 ± 0.32	0.51 ± 0.26	0.35 ± 0.15	0.14 ± 0.06	11.18 ± 1.86	1.10 ± 0.50
	JPS105	5	4.6 ± 0.3	3.6 ± 0.2	0.59 ± 0.47	1.15 ± 0.53	0.30 ± 0.14	0.25 ± 0.11	14.36 ± 3.28	1.37 ± 0.77
	JPS006	5	4.3 ± 0.3	3.5 ± 0.2	0.22 ± 0.15	0.36 ± 0.37	0.16 ± 0.08	0.09 ± 0.11	7.58 ± 2.16	1.02 ± 0.31
	JPS106	4	4.5 ± 0.4	4.0 ± 0.2	0.17 ± 0.19	0.18 ± 0.08	0.23 ± 0.09	0.03 ± 0.02	5.81 ± 4.41	0.76 ± 0.55
Malaysia	MYS001	3	4.3 ± 0.3	3.8 ± 0.2	0.24 ± 0.22	0.30 ± 0.27	0.20 ± 0.11	0.12 ± 0.03	3.02 ± 0.60	NA
	MYS101	2	4.3 ± 0.3	3.8 ± 0.3	0.07 ± 0.05	0.05 ± 0.06	0.05 ± 0.03	0.06 ± 0.04	3.35 ± 0.61	NA
	MYS201	1	4.3 ± 0.1	3.9 ± 0.1	0.10 ± 0.02	0.11 ± 0.03	0.11 ± 0.03	0.01 ± 0.02	0.53 ± 0.17	0.80 ± 0.15
	MYS202	1	4.4 ± 0.1	3.9 ± 0.1	0.15 ± 0.06	0.15 ± 0.02	0.22 ± 0.15	0.02 ± 0.03	0.50 ± 0.22	0.83 ± 0.13
	MYS005	2	5.3 ± 0.5	4.0 ± 0.7	1.36 ± 0.50	1.02 ± 0.19	0.06 ± 0.02	1.30 ± 0.17	1.84 ± 0.27	2.01 ± 0.30
	MYS105	2	4.8 ± 0.2	3.7 ± 0.1	0.78 ± 0.30	0.83 ± 0.22	0.04 ± 0.02	1.42 ± 0.13	1.52 ± 0.27	1.66 ± 0.28
Mongolia	MNS001	3	6.2 ± 0.5	5.3 ± 0.6	NA	NA	NA	NA	NA	NA
	MNS002	3	5.8 ± 0.6	5.0 ± 0.6	NA	NA	NA	NA	NA	NA
Philippines	PHS002	4	5.8 ± 0.6	4.8 ± 0.6	15.57 ± 4.13	10.53 ± 3.79	3.90 ± 1.21	1.60 ± 1.62	0.19 ± 0.46	0.28 ± 0.19
	PHS102	5	4.4 ± 0.3	3.8 ± 0.2	0.85 ± 1.29	0.31 ± 0.14	0.35 ± 0.17	0.26 ± 0.18	5.31 ± 1.26	0.61 ± 0.39
	PHS001	2	5.3 ± 0.3	4.2 ± 0.2	17.05 ± 7.78	5.07 ± 1.37	0.70 ± 0.47	2.24 ± 1.00	0.15 ± 0.14	0.19 ± 0.14
	PHS003	1	5.2 ± 0.2	5.0 ± 0.1	7.11 ± 1.18	0.86 ± 0.15	0.21 ± 0.03	0.39 ± 0.06	1.68 ± 0.35	0.35 ± 0.09
R. of Korea	KRS003	2	4.9 ± 0.2	4.0 ± 0.1	0.38 ± 0.36	0.17 ± 0.12	0.10 ± 0.04	0.08 ± 0.06	3.22 ± 0.49	0.31 ± 0.15
Russia	RUS003	2	6.3 ± 0.4	4.8 ± 0.7	17.29 ± 5.42	4.35 ± 1.51	0.23 ± 0.10	0.14 ± 0.04	0.13 ± 0.14	0.04 ± 0.03
	RUS002	2	5.7 ± 0.9	4.6 ± 0.9	15.66 ± 9.67	3.27 ± 1.87	0.43 ± 0.52	0.08 ± 0.04	1.05 ± 1.46	0.22 ± 0.24
	RUS102	1	4.8 ± 0.3	3.9 ± 0.6	4.24 ± 4.29	1.04 ± 1.09	0.36 ± 0.39	0.11 ± 0.05	8.30 ± 5.35	1.42 ± 0.56
	RUS001	0 (1)	ND	ND	ND	ND	ND	ND	ND	ND
	RUS101	0 (1)	ND	ND	ND	ND	ND	ND	ND	ND
	RUS201	1 (1)	7.4 ± 0.2	6.9 ± 0.1	100.36 ± 17.66	5.94 ± 1.90	1.98 ± 1.42	0.02 ± 0.02	NA	NA
	RUS004	2	5.2 ± 0.3	4.2 ± 0.7	10.28 ± 7.72	3.11 ± 1.22	0.38 ± 0.27	0.14 ± 0.05	0.71 ± 0.89	0.30 ± 0.07
Thailand	THS004	6	6.4 ± 0.5	5.5 ± 0.5	13.66 ± 10.14	7.79 ± 13.70	0.20 ± 0.36	0.19 ± 0.19	0.08 ± 0.08	7.43 ± 13.00
	THS104	4	5.1 ± 0.6	4.1 ± 0.3	2.38 ± 2.75	1.04 ± 0.75	0.03 ± 0.03	0.17 ± 0.13	1.26 ± 1.41	7.26 ± 14.19
Vietnam	VNS002	0 (1)	ND	ND	ND	ND	ND	ND	ND	ND
	VNS102	0 (1)	ND	ND	ND	ND	ND	ND	ND	ND

(), number of surveys including pre survey in 1999.
Mean ± SD.
NA represents "not analysed".
ND indicates no official data since 2000.

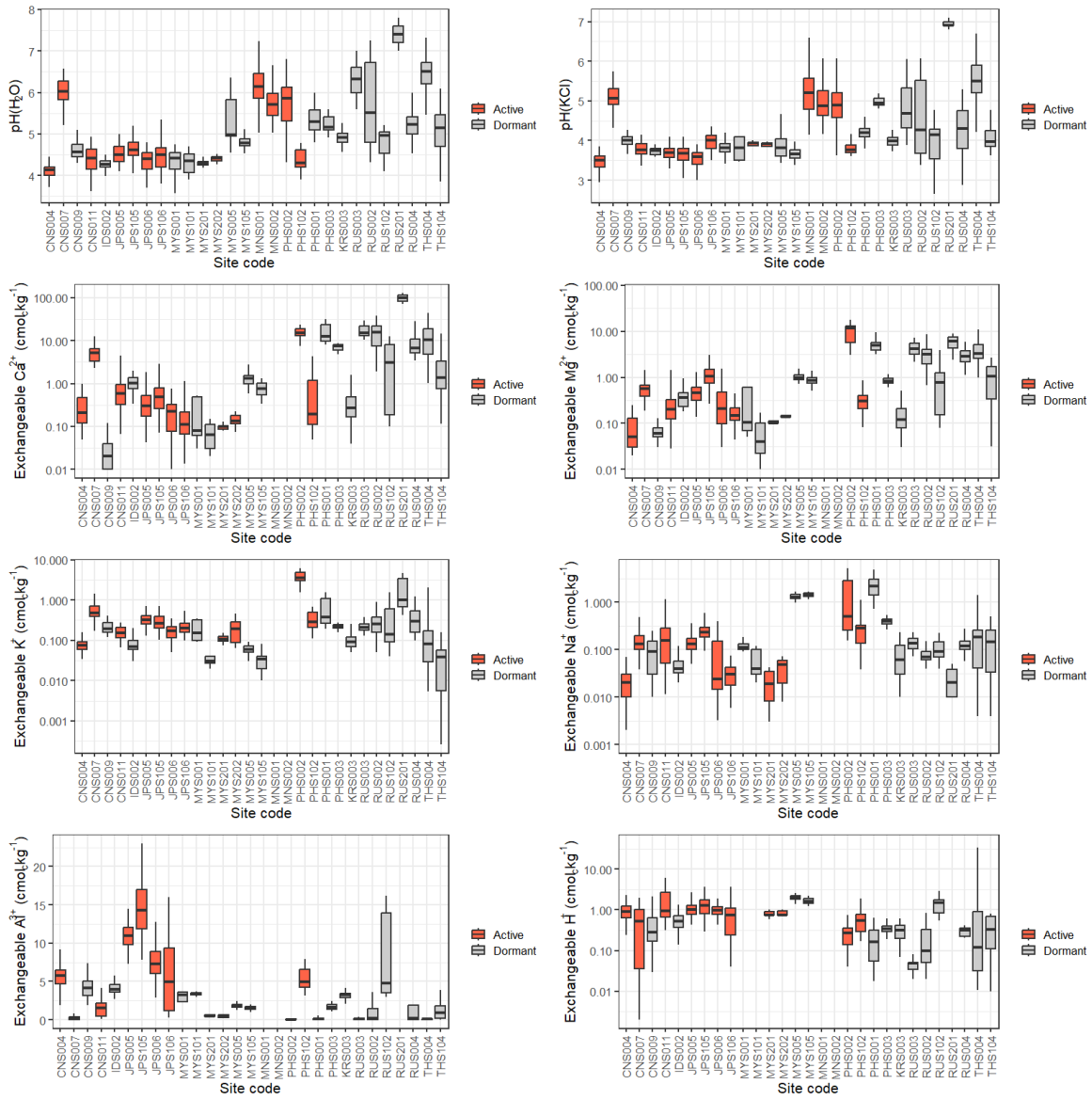

Figure 5.3.1. Statistics of soil chemical properties over the entire monitoring period at each EANET site. The horizontal line within each box represents the median; the upper and lower edges of the box indicate the third and first quantiles, respectively; and the upper and lower whiskers denote the maximum and minimum values. The reddish color indicates active sites where monitoring was conducted from 2019 to 2024.

Mean soil pH and concentrations of exchangeable cations are shown in Table 5.3.2 and Figure 5.3.1. Mean pH(H_2O) ranged very widely from 4.1 to 7.4 among EANET sites. Soil pH(H_2O) of middle-latitude site (China and Japan) tended lower compared to other sites. Variability within the same country (if there are multiple sites in a country) was also large. Similarly, pH(KCl) and soil exchangeable cations ranged widely; the average were 3.5 ~6.9 for pH(KCl), 0.03 ~ 100.36 $cmol_c$ kg^{-1} for Ca^{2+}, 0.05 ~ 10.53 $cmol_c$ kg^{-1} for Mg^{2+}, 0.03 ~ 3.90 $cmol_c$ kg^{-1} for K^+, 0.01 ~ 2.24 $cmol_c$ kg^{-1} for Na^+, 0.08 ~ 14.36 $cmol_c$ kg^{-1} for Al^{3+}, 0.04 ~ 7.43 $cmol_c$ kg^{-1} for H^+.

Figure 5.3.2 shows soil pH and exchangeable cations among different soil types. Among the seven soil types identified at EANET soil monitoring sites, Gleysols had the highest pH(H_2O) and pH(KCl). Gleysols generally occur in poorly drained locations saturated with groundwater, resulting in reduced soil condition (IUSS Working Group WRB, 2015). This soil type was observed at the Solar Observatory site in Russia (RUS201). In contrast, Andosols and Nitisols showed the lowest values.

Andosols are typically derived from weathered volcanic ash and are rich in active aluminum. This soil type was observed at the Yamato site in Japan (JPS106). Nitisols have a clay-rich subsurface horizon and relatively low cation exchange capacity (CEC). This soil type was observed at the Up Quezon Land Grant site in Philippines (PHS102). Consistent with soil pH, exchangeable base cations such as Ca^{2+} and Mg^{2+} were higher in Gleysols and lower in Andosols and Nitisols. The soil type at nearly half of the sites has not been specified according to the international soil classification system (Table 5.3.1). If soil classification is completed across all EANET sites, the relationships between soil type and soil chemical properties will become clearer.

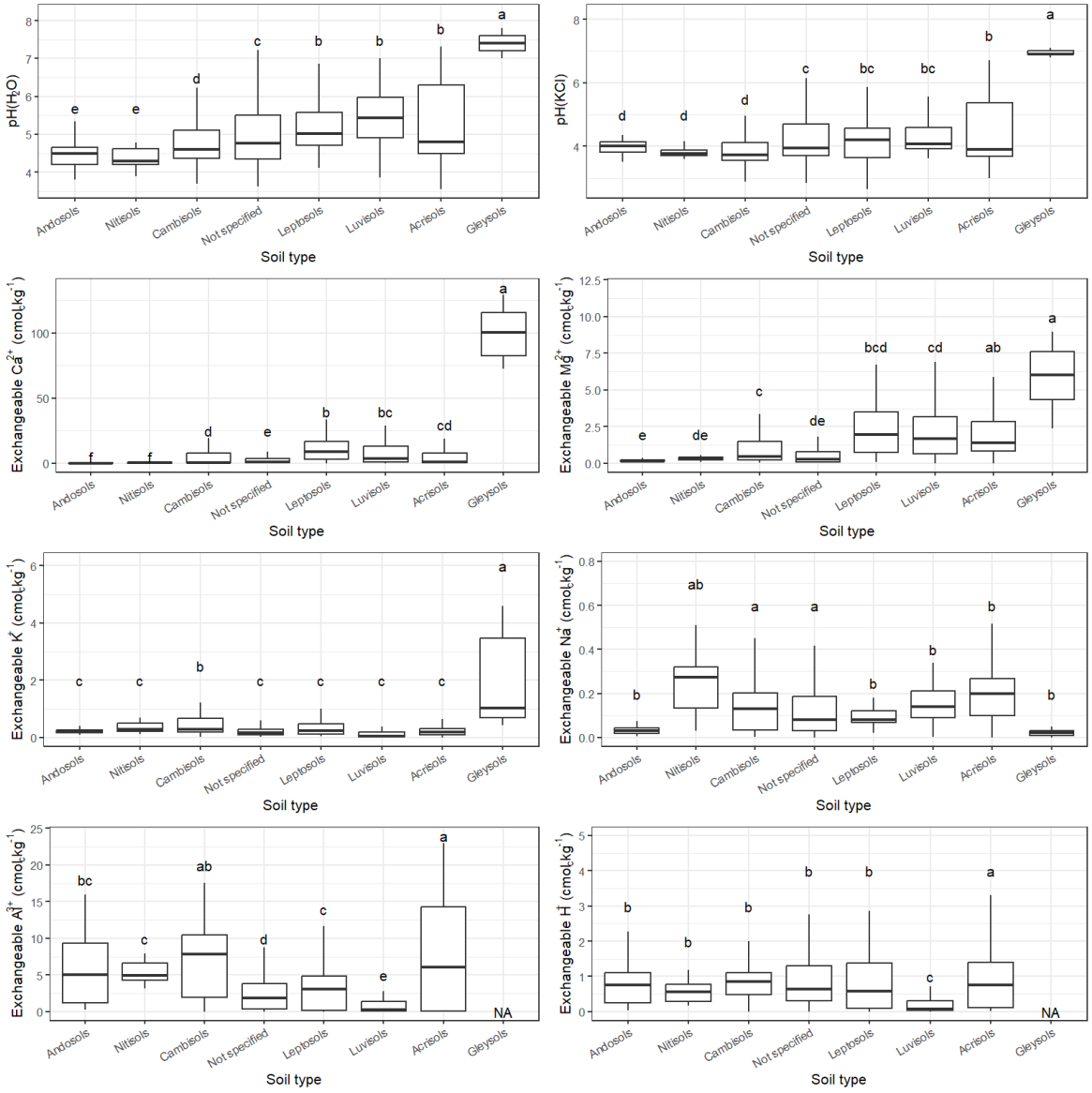

Figure 5.3.2. Soil pH and chemical properties among soil types. Different alphabets represent significant difference ($p < 0.05$, Tukey HSD test). Explanations for box plot are the same as Fig. 5.3.1.

Forest trees affect soil chemical properties through litter input and decomposition of organic matter (Berg and McClaugherty, 2014). Figure 5.3.3 shows differences in pH and soil chemical properties among forest types. In this report, forest types are classified based on combinations of [evergreen or deciduous] and [coniferous or broad-leaved], resulting in four categories. Among these forest types, deciduous coniferous forests exhibit the highest soil pH(H_2O) and pH(KCl), as well as exchangeable base cations such as Ca^{2+}, Mg^{2+}, and K^{+}. This category mainly consists of *Larix sibirica*, which is distributed in Mongolia and Russia. In contrast, evergreen coniferous forests showed the lowest soil

pH(H_2O) and pH(KCl), along with lower concentrations of exchangeable base cations. This category mainly includes species of *Pinus* and *Chamaecyparis*. In Japanese forests, the litter of these species is characterized by low decomposability; this suggests that the slow decomposition process contributes to high humic acid content and low soil pH (Takahashi et al., 1999; Oyanagi et al., 2002). At 11 of the 33 sites, forest type has not been specified because forest surveys have not been conducted. If surveys are carried out at more sites, forest types can be classified more precisely. Such information on forest characteristics (including not only tree species but also stand age, and whether forests are natural or planted) will help clarify nutrient interactions between trees and soils.

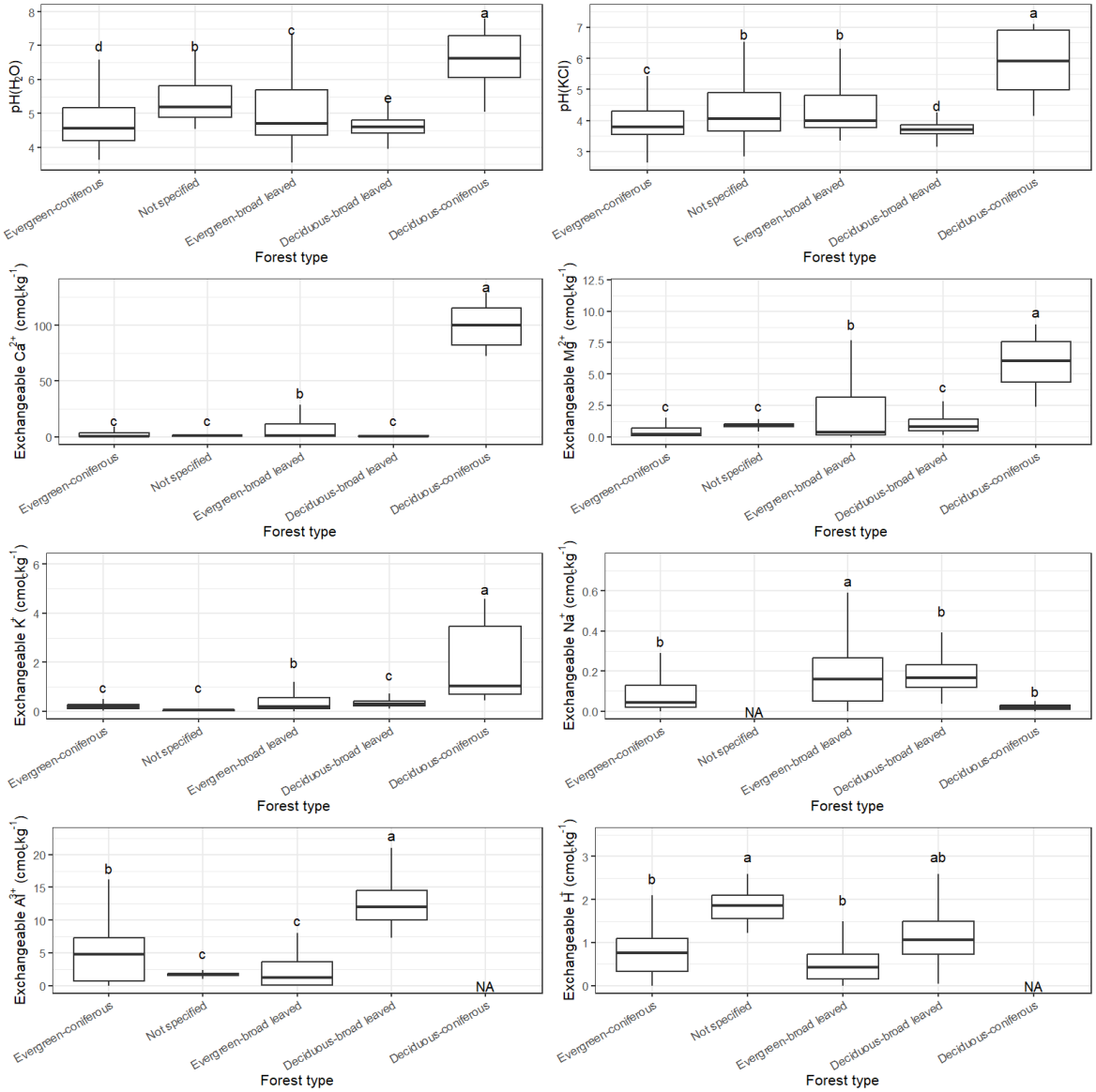

Figure 5.3.3. Soil pH and chemical properties among forest types. Different alphabets represent significant difference ($p < 0.05$, Tukey HSD test). Explanations for box plot are the same as Fig. 5.3.1.

Relationships between mean annual precipitation and soil pH and other soil chemical properties are shown in Figure 5.3.4. The correlations between precipitation and soil pH(H_2O) and pH(KCl), as well as exchangeable base cations such as Ca^{2+} and Mg^{2+}, were negative, indicating that soil pH and exchangeable base cation concentrations are lower at sites with higher precipitation. In general, high precipitation induces chemical weathering of soil minerals and leaching of base cations, resulting in soil acidification and lower soil pH (Breemen et al., 1984).

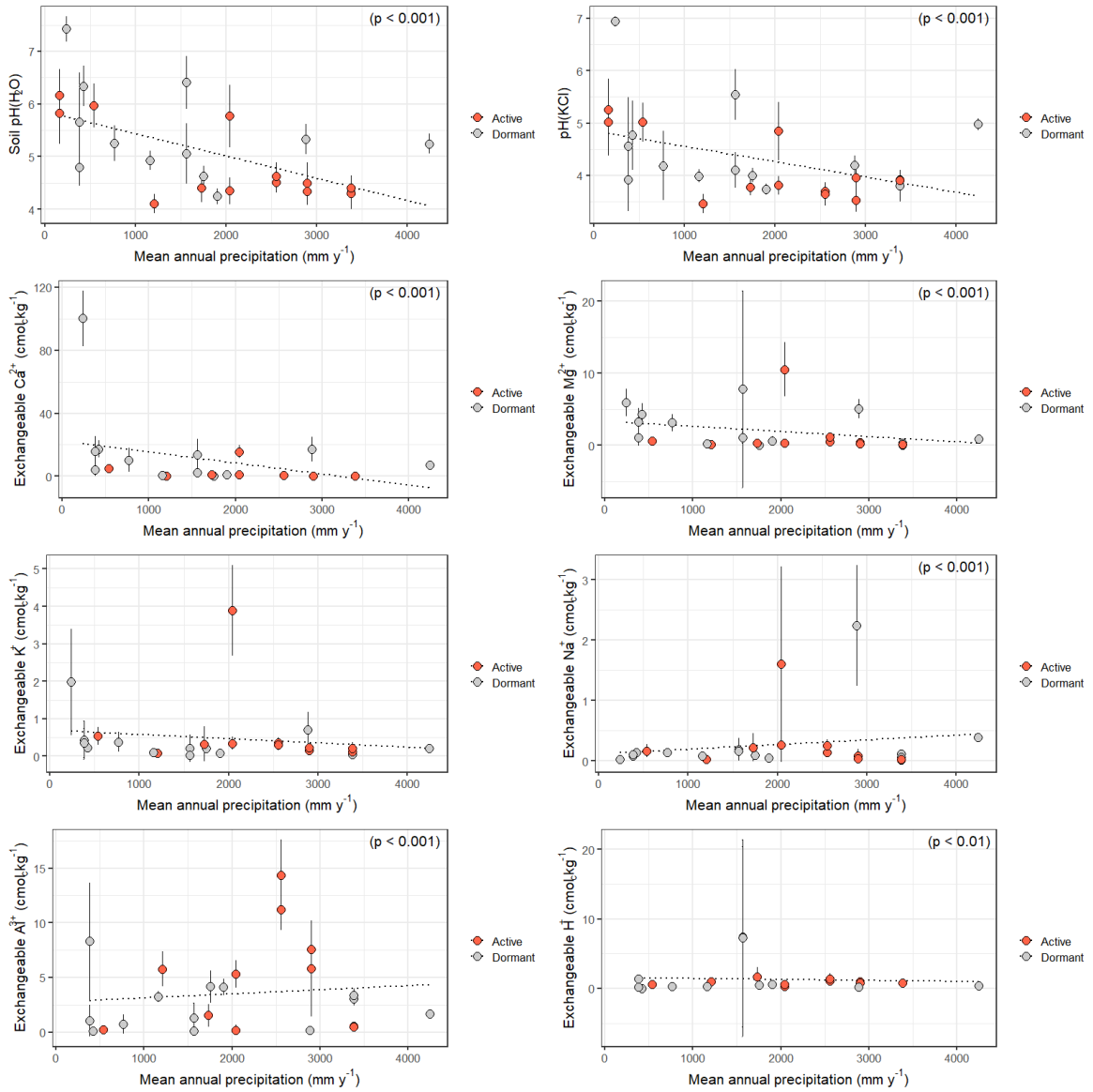

Figure 5.3.4. Relationship between mean annual precipitation and soil pH as well as soil chemical properties of each monitoring site.

To elucidate which factor is most important in controlling soil chemical properties among the three factors --- soil type, forest type, and mean annual precipitation--- PLS-R (partial least squares regression) analysis was performed. This method is similar to multiple regression analysis but is suitable for handling explanatory variables with multicollinearity. The results showed that soil type was the dominant factor controlling variations in Na^+, Al^{3+}, and H^+ (Table 5.3.3). Forest type was the dominant factor for Ca^{2+}, Mg^{2+}, and K^+, while mean annual precipitation was the dominant factor for $pH(H_2O)$, pH(KCl), Ca^{2+}, Mg^{2+}, and Na^+. Soil is formed from the accumulation and decomposition of forest litter, as well as the weathering products of bedrock. The annual photosynthetic rate of the forest, which determines litter production, depends on the amount of annual precipitation. Annual precipitation reflects not only water supply and leaching, but also the average temperature. Therefore, these results suggest that soil formation processes, forest composition, and climatic conditions, as represented by mean annual precipitation, influence soil chemical properties.

Table 5.3.3 Results of PLS-R: VIP*s for soil chemical properties

	$pH(H_2O)$	pH(KCl)	Ca^{2+}	Mg^{2+}	K^+	Na^+	Al^{3+}	H^+
- Soil type	0.62	0.83	0.93	0.54	0.39	**1.22**	**1.18**	**1.51**
- Forest type	0.46	0.73	**1.00**	**1.04**	**1.44**	0.71	0.92	0.81
- Mean annual precipitation	**1.55**	**1.34**	**1.07**	**1.27**	0.87	**1.00**	0.88	0.27

*, VIP (variable importance for projection) means the strength of each explaining variable.

5.3.2 Temporal changes in soil $pH(H_2O)$ with respect to atmospheric environment

The previous section presented that inherent soil chemical properties at EANET sites vary widely, influenced by soil formation processes, forest composition, and climatic conditions. This suggests that the sensitivity and response characteristics of soils to the external environment differ among sites. As anthropogenic atmospheric deposition in EANET countries has decreased over the past decade, corresponding changes in soil chemical properties are expected. This section examines the temporal variations in soil $pH(H_2O)$ in relation to atmospheric monitoring data and investigates the relationship between atmospheric chemistry and soil $pH(H_2O)$.

The target sites were selected based on the following three criteria:
- Presence of a corresponding atmospheric monitoring station.
- Availability of soil monitoring data since 2000.
- Conductance of soil monitoring surveys on at least two occasions.

Based on these criteria, monitoring data from 22 sites across 9 countries were analyzed. Nine sites (MYS005, MYS105, PHS003, RUS102, RUS001, RUS101, RUS201, VNS002, and VNS102) were excluded from the analysis.

Figures 5.3.5a and b illustrate the temporal changes in $pH(H_2O)$ at each EANET site. The background bands represent the trends in annual wet deposition of nss-SO_4^{2-}, as observed at the atmospheric monitoring stations corresponding to each soil monitoring site. At most sites, the temporal change in soil $pH(H_2O)$ appears to fluctuate in accordance with the trends in acid deposition. The annual wet deposition of nss-SO_4^{2-} has shown a downward trend at sites in China, Japan, the Philippines (Metro Manila), and the Republic of Korea. Consistent with this decrease, the $pH(H_2O)$ at sites CNS004, CNS009, CNS011, JPS006, and JPS106 exhibited an increasing trend (Figure 5.3.5a). Although soil $pH(H_2O)$ is theoretically expected to increase in response to this atmospheric trend, the observed temporal changes did not necessarily follow this pattern at several sites (e.g., CNS007, PHS001, KRS003, RUS002, and RUS003). These results suggest that the impact of acid deposition on soil chemical properties is complex, as it reflects not only the neutralization reactions of soil minerals but also numerous other processes, including interactions between atmospheric deposition, forest vegetation, and the litter layer (Larssen and Carmichael, 2000; Berg and McClaugherty, 2014).

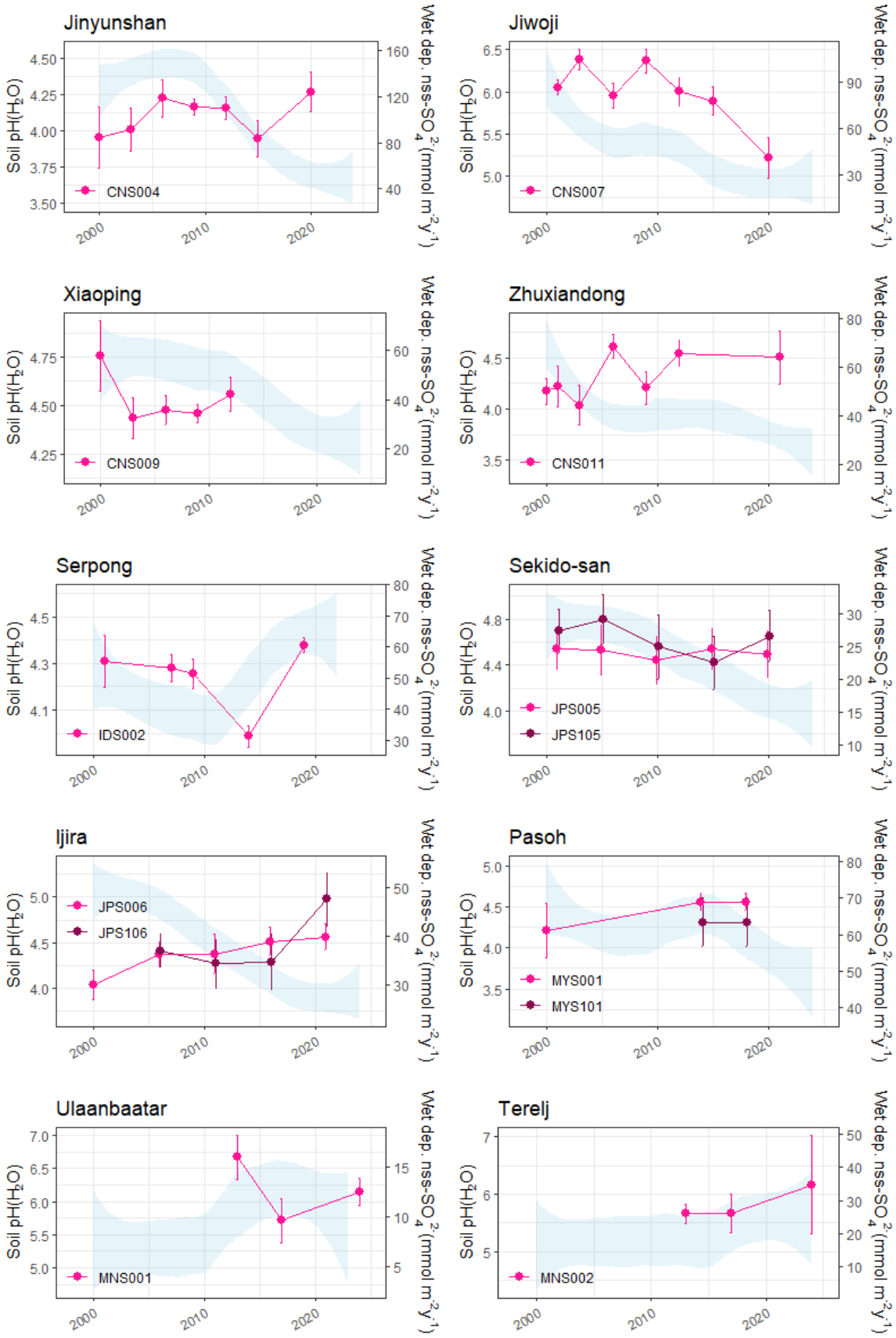

Figure 5.3.5a. Temporal changes in soil pH(H_2O) in relation to wet deposition of nss-SO_4^{2-}. The line charts represent the soil pH(H_2O) for each survey year. The shaded bands represent the variation in wet deposition of nss-SO_4^{2-} as determined by LOESS (locally weighted scatter plot smoothing) with a 95% confidence interval.

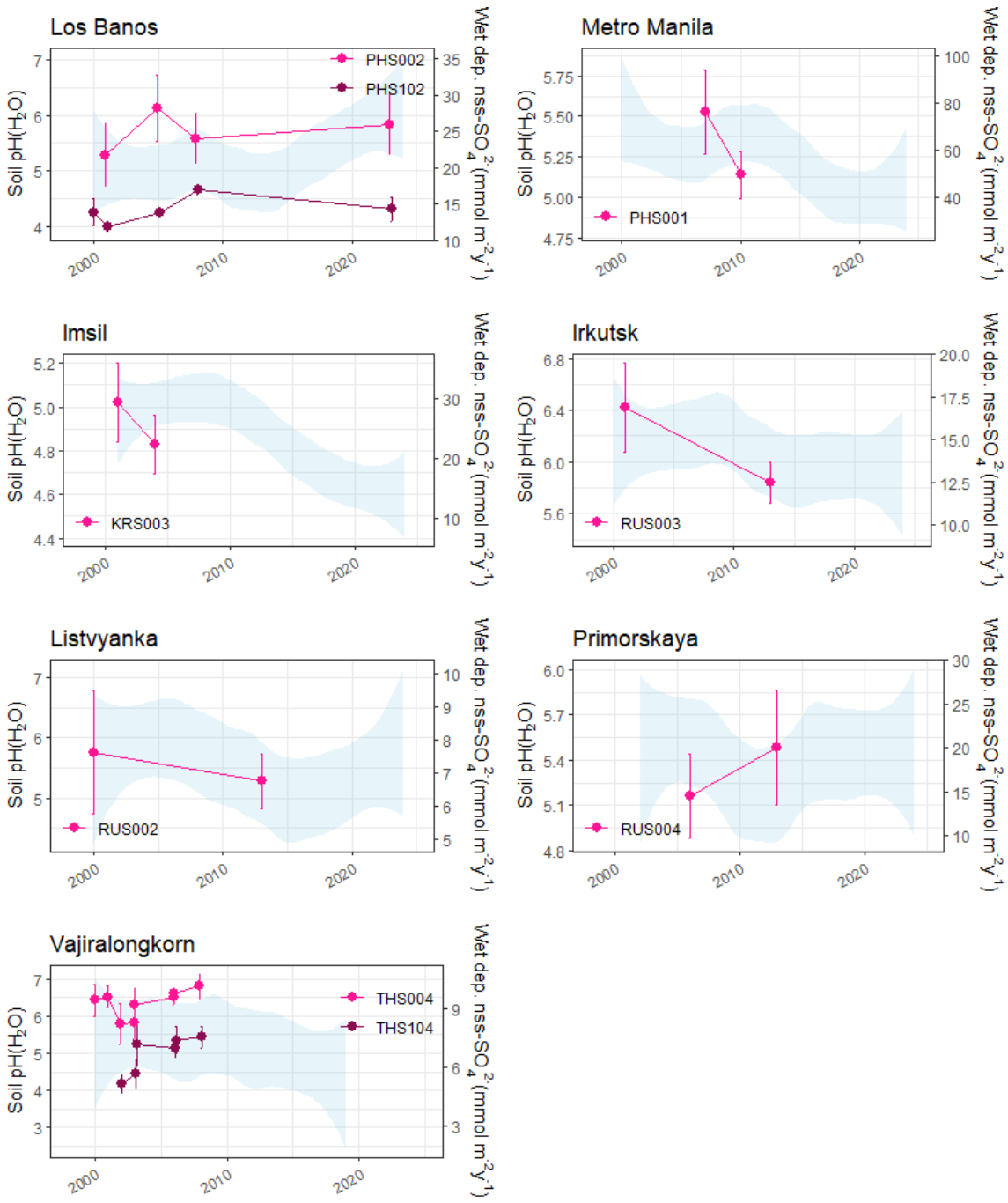

Figure 5.3.5 b. Temporal changes in soil pH(H_2O) with wet deposition nss-SO_4^{2-}. The line charts represent the soil pH(H_2O) for each survey year. The shaded bands represent the variation in wet deposition of nss-SO_4^{2-} as determined by LOESS (locally weighted scatter plot smoothing) with a 95% confidence interval.

To examine the relationships between soil chemical properties and atmospheric deposition, a regression analysis was conducted between soil pH(H_2O) and the wet deposition of pH, nss-SO_4^{2-}, nss-Ca^{2+}, NH_4^+ and NO_3^- (Table 5.3.4). A positive (+) correlation indicates that soil pH(H_2O) follows the fluctuations in wet deposition; that is, an increase in the wet deposition of a specific constituent is accompanied by an increase in soil pH(H_2O). Ideally, increase in nss-SO_4^{2-}, NH_4^+, and NO_3^- − which act as acidifying substances in the soil (Baba and Okazaki, 1998) − should lead to a decrease in soil pH(H_2O). However, the sign of the correlation varied between positive and negative among sites, suggesting that the soil's response to wet deposition is not uniform. In China, it has been

suggested that nss-Ca^{2+} is derived from both calcareous material in desert dust and anthropogenic emission sources, and that, this nss-Ca^{2+} contributes to neutralizing acid deposition and mitigating soil acidification (Larssen and Carmichael, 2000; Duan et al., 2016). These results suggest that, beyond the direct interaction between atmospheric agents and soil, the inherent diversity in soil chemical characteristics across sites and the complexity of soil reactions to atmospheric acidifying substances contribute to these varied responses.

Table 5.3.4 Slope of correlation between soil pH(H_2O) and items of wet deposition

Country	Site code	pH	nss-SO_4^{2-}	nss-Ca^{2+}	NH_4^+	NO_3^-
China	CNS004	+	ns	+	ns	+
	CNS007	−	+	+	+	+
	CNS009	+	−	−	−	−
	CNS011	+	−	−	−	ns
Indonesia	IDS002	−	ns	ns	−	−
Japan	JPS005	ns	ns	ns	ns	ns
	JPS105	−	+	+	+	+
	JPS006	+	−	−	−	−
	JPS106	+	−	+	−	−
Malaysia	MYS001	+	−	ns	−	+
	MYS101	ns	ns	ns	ns	ns
Mongolia	MNS001	+	+	+	+	−
	MNS002	+	ns	ns	ns	−
Philippines	PHS002	ns	−	−	−	−
	PHS102	−	+	−	+	−
	PHS001	−	+	+	−	−
R. of Korea	KRS003	+	+	−	+	−
Russia	RUS003	+	+	+	+	+
	RUS002	ns	ns	ns	ns	ns
	RUS004	+	−	−	−	−
Thailand	THS004	+	ns	−	ns	ns
	THS104	+	−	−	ns	ns

+, −, and ns represent significant-positive, significant-negative and not significant correlations, respectively.

5.3.3 Summary

Soil monitoring data from 2000 to 2024 were reviewed in this section. Section 5.3.1 highlighted the diverse soil characteristics across EANET sites, suggesting that the primary factors controlling this widespread variation include soil formation processes, forest composition, and climatic conditions. In Section 5.3.2, temporal changes in soil pH(H_2O) were presented alongside deposition parameters; the results suggested that soil responses do not necessarily parallel the trends in atmospheric deposition. Given the diverse distribution of soil characteristics among EANET sites, the reaction processes likely vary by site. However, at a considerable number of sites, soil monitoring has not been conducted frequently enough over the past 25 years. This implies that the current framework may be insufficient for detecting the ecological impacts resulting from changes in the atmospheric environment. As this monitoring system provides valuable data for understanding the effects of climate change on ecosystems, it is essential that soil monitoring to be continued more intensively and consistently.

5.4. Forest vegetation

5.4.1 Characteristics of monitoring stands

Vegetation monitoring has been conducted at 29 sites in 9 countries since 2000. The basic survey was principally carried out for the initial objectives (namely, establishment of baseline data and early detection of possible impact) in the participating countries in accordance with the Technical Documents for Soil and Vegetation Monitoring in East Asia (EANET 2000). These are performed in the same stand as soil monitoring and detailed metadata are shown in Table 5.3.1. However, there is a large variation in the content and frequency of surveys among sites. Regarding vegetation monitoring, it was assumed that comprehensive forest survey (General description of forest; GDF), tree decline survey (Observation of tree decline; OTD), and understory vegetation survey would be conducted. However, the only sites that have been surveyed more than once since 2015 are those in China and Japan. There are four monitoring sites that can track the diameter at breast height (DBH) growth of standing trees in China, two at Jinyunshan (CNS004), and Dabagou (CNS007) and Xiaoping (CNS009). Records from 2003 to 2024 are registered for the two sites of Jinyunshan. There also are four monitoring sites in Japan. Records have been registered for two sites at Banryu (JPS008, 108) since 2001, but monitoring of these sites has ended in 2018, and they have been replaced with two new sites at Happo (JPS005, 105). For PRSAE5, only EANET data should be used in the main analysis. However, due to the prospect of continued observations at this site, data from domestic monitoring conducted at Happo prior to registration were presented. Records of Ijira (JPS006) and Yamato (JPS106) have been registered since 2006, and the data up to 2021 are available. Typically, trees subject to GDF are individually identified and recorded every 3 to 5 years. OTD is conducted every year for some GDF target trees, but the number of trees surveyed is small.

As shown in previous chapters, there has been a decreasing trend in anthropogenic atmospheric deposition over the last decade, so it is necessary to verify whether this has affected vegetation properties. In this section, temporal changes in DBH increase rate of individual trees and the total trunk cross-sectional area at breast height (BA) of the eight sites in Japan and China were analyzed. This is because these eight sites were the only sites where data was recorded in a continuously comparable manner. Firstly, the tree dynamics of each site will be described. Then, we consider what factors can explain their dynamics.

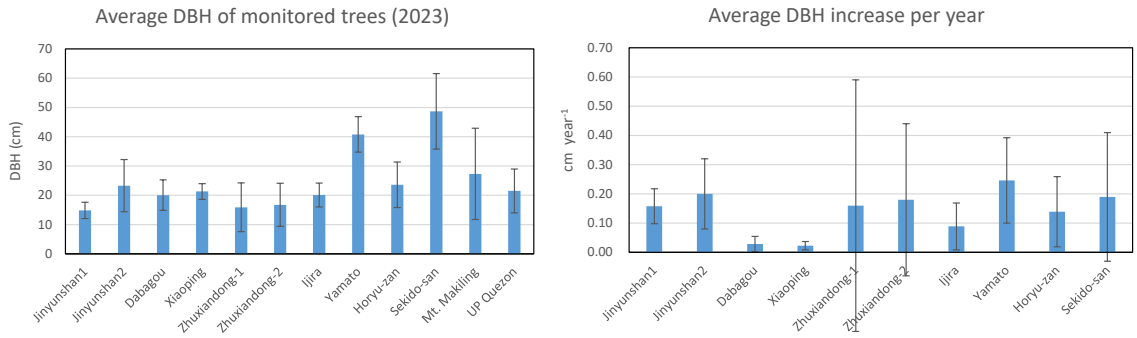

Figure 5.4.1 Average DBH of monitored trees for each stand (left) and the increase in DBH over the last 5 years (right) in the tree decline survey (OTD). Vertical lines indicate standard deviation. The trees included in the OTD survey were individually identified; the survey area covered 1,000 m² (the large circle), and trees with a DBH greater than 18 cm were measured. Since individual identification has not been maintained across surveys at Mt. Makiling and UP Quezon, DBH growth are not presented.

5.4.2 Stand dynamics

(1) Sekido-san (JPS005)

This site is located in the central part of a peninsula that juts (protrudes?) into the Sea of Japan in central Honshu. It is presumed to be more susceptible to transboundary air pollution from the continent than to local air pollution. The site consists of a deciduous broad-leaved forest dominated

by *Fagus crenata* and comprising approximately 16 tree species. Data on the DBH from 2001 to 2020 for GDF and OTD were analyzed (Fig. 5.4.1). The number of trees included in the GDF was 45 in 2001. In 2005, 45 trees were confirmed, and in 2015, 95 trees were registered. Subsequently, the death of shrubs was confirmed, and by 2020, the number of trees included in the survey had decreased to 89. The primary cause of death is estimated to be the shading from large trees, though physical damage from snow accumulation was also considered a possibility. The annual increase in DBH of individual trees has shown a rising trend since 2015, but there is significant variation among individuals (Fig. 5.4.2a, b). The total basal area (BA) of the trees surveyed for GDF increased until 2015 and has plateaued since then (Fig. 5.4.2c).

(2) Horyu-zan (JPS105)

This site is located at the tip of a peninsula that juts into the Sea of Japan in central Honshu. It is presumed to be susceptible to transboundary air pollution. The site consists of a deciduous broad-leaved forest dominated by *Fagus crenata* and comprising approximately 22 tree species. DBH data for GDF and OTD at this site was analyzed from 2001 to 2020 (Fig. 5.4.1). The number of trees included in the GDF survey was 156 in 2001. In 2010, 237 trees were identified, and 281 trees were registered in 2015. In 2020, the survey included 212 trees. The fluctuation in the number of surveyed trees is thought to be primarily due to shrubs with a DBH of 5 cm or less and is likely influenced by variations in survey conditions. The main cause of death was presumed to be competition with neighboring trees. The annual increase in DBH of individual trees showed no significant trends throughout the survey period, and no significant changes over time were observed (Fig. 5.4.2d, e). The total BA of the GDF survey trees increased, suggesting that the stand is maturing stably (Fig. 5.4.2f).

(3) Ijira (JPS006)

This site is located in the inland region of central Honshu, an area susceptible to urban air pollution in Japan. It is a young cypress plantation, and the stand consists of almost one species, *Chamaecyparis obtusa*. At this site, DBH data from 2006 to 2021 were analyzed for GDF and OTD. A total of 121 trees were included in the GDF analysis in 2006 (Fig. 5.4.1). Between 2006 and 2011, 37 trees were thinned. By 2016, 26 trees had been recruited, and 3 had died; thus, the total number of trees in the study was 109. By 2021, the sample included 115 trees. In the OTD survey, DBH was recorded for 8 trees in 2006 and 12 new trees were recorded from 2011. The annual increase in DBH of individual trees showed a decreasing trend (Fig. 5.4.2g, h). The total BA of the trees surveyed by GDF decreased slightly after thinning in 2011, but has increased steadily since 2016 (Fig. 5.4.2i), suggesting that forest growth continues even after thinning. This site has a high planting density, and the growth data indicates that growth inhibition due to inter-individual interactions continues even after thinning, thus suppressing the increase in DBH of individual trees.

(4) Yamato (JPS106)

This site is located in the inland region of central Honshu and is expected to be susceptible to the influence of urban atmosphere in Japan. It is a matured cypress plantation, and the stand consists of one species, *Chamaecyparis obtusa*. At this site, DBH data from 2006 to 2021 were analyzed for GDF and OTD. The GDF analysis included 48 trees from 2006. Thinning was conducted on 19 trees between 2011 and 2016. By 2016, no trees had been recruited, and 4 had died, and by 2021, 6 more had died, leaving 19 trees in the stand. In the OTD survey, DBH was recorded for 20 trees in 2006, and 10 trees were replaced during the period. Consequently, the remaining 10 were measured continuously. The annual increase in DBH of individual trees showed a decreasing trend (Fig. 5.4.2j, k). The total BA of trees in the GDF survey decreased significantly in 2016 due to thinning, suggesting that the impact of thinning was very large (Fig. 5.4.2l). Furthermore, total BA has continued to show a decreasing trend since then. On the other hand, the average DBH increase was

the highest among the survey sites (Fig. 5.4.1). This suggested that thinning promoted the increase in DBH of individual trees.

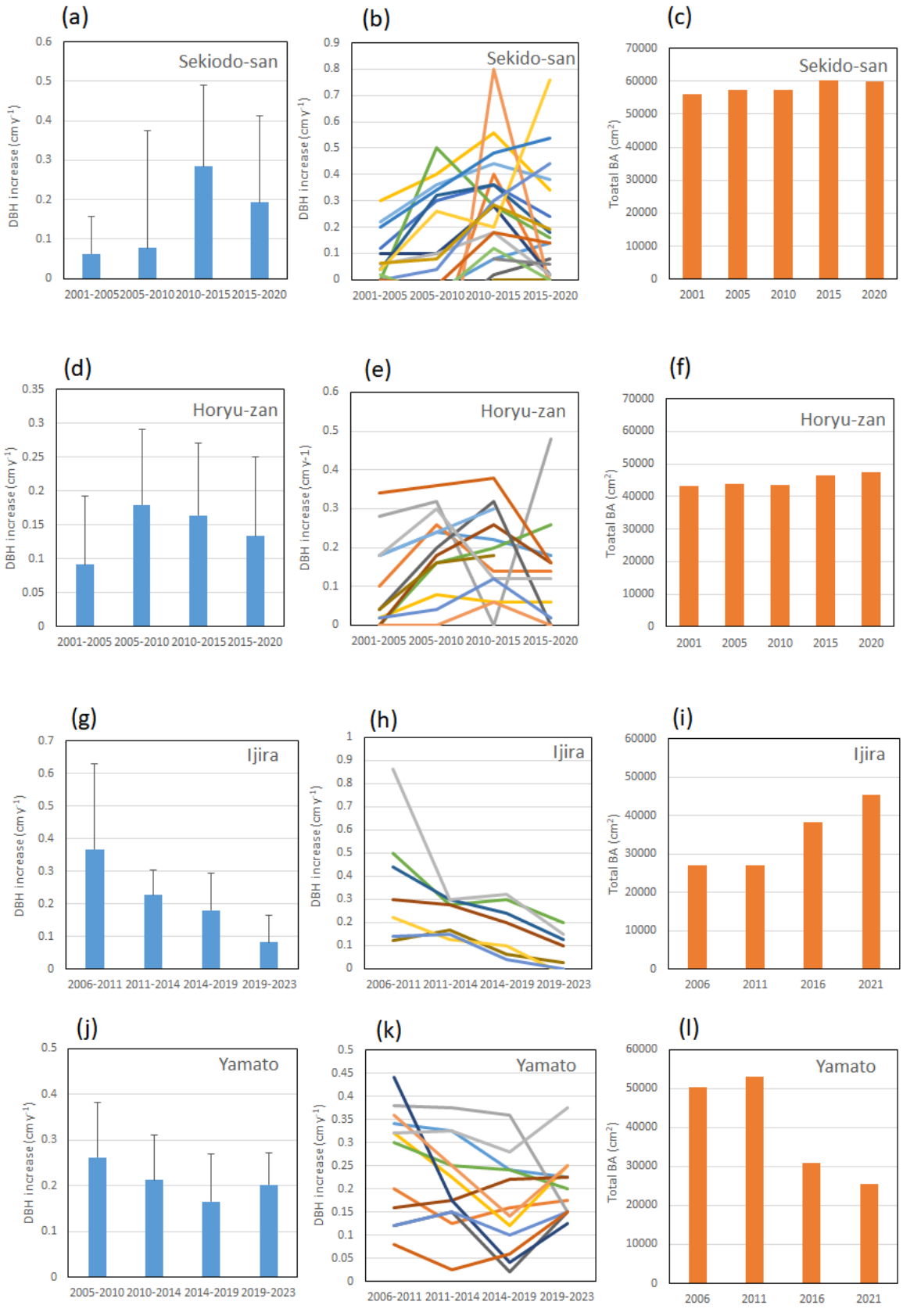

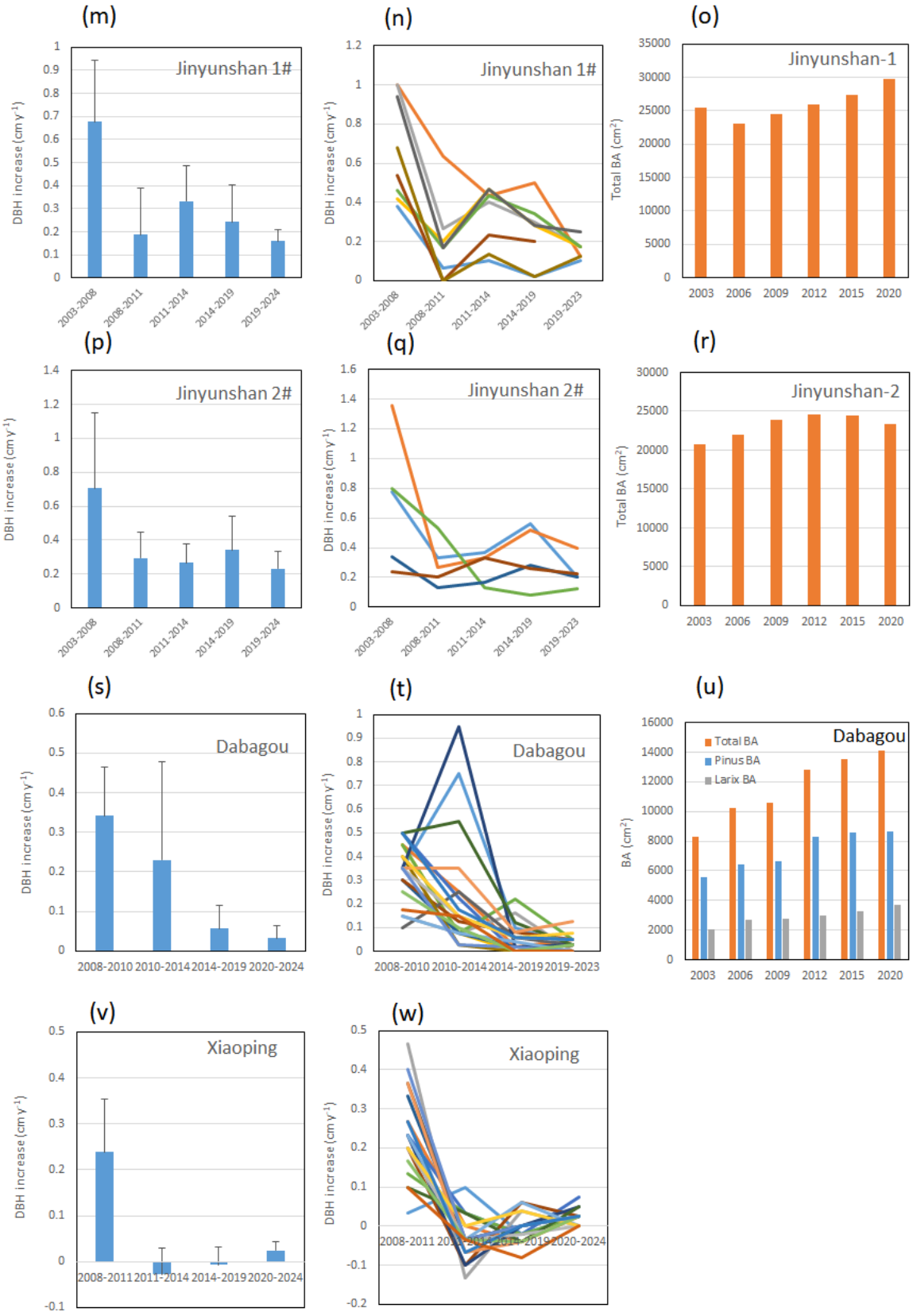

Figure 5.4.2 Average annual increase in DBH (left column) of OTD, DBH increase for each individual tree of OTD (middle column), and changes in total BA for each year at each GDF survey (right column).
Vertical lines indicate standard deviation. In the graphs showing the OTDs in the middle row (b, e, h, k, n, q, t, w), each colored line represents a different individual.

(5) Jinyunshan (CNS004)
Jinyunshan is located in the inland area of China and was selected as a rural site. The study area is set up with two stands (Jinyunshan-1, Jinyunshan-2), and Jinyunshan-1 is an evergreen mixed forest dominated by *Castanopsis carlesii* var. *spinulosa, Pinus massoniana* and *Symplocos setchuenensis* and is composed of approximately 14 tree species. Jinyunshan-2 is an evergreen broad-leaved forest composed of approximately 10 tree species including *Castanopsis fargesii*, *Elaeocarpus japonicus* and *Machilus pingii*. At both sites, DBH data from 2003 to 2019 were analyzed for GDF and OTD.

At Jinyunshan-1, the number of target trees of GDF were 104 in 2003. By 2006, 11 trees had been cut down and 11 trees had died. By 2015, one tree had been recruited and 5 trees had died, bringing the number of trees surveyed to 78. By 2020, even more shrubs had died, so the number of trees to 67. The main cause of death was presumed to be competition with neighboring individuals. In the OTD survey, 10 trees were recorded in 2003, and 1 trees died in 2016, and 1 each died in 2023 and 2024, leaving a total of 7 trees in the survey. The annual increase in DBH of individual trees was fairly variable throughout the period (Fig. 5.4.2m, n), but the average DBH increase rate was the highest among the monitoring sites (Fig. 5.4.1). The total BA of the trees surveyed by GDF decreased slightly in 2006 after thinning and continued to increase through 2020 (Fig. 5.4.2o).

At Jinyunshan-2, the number of target trees of GDF were 71 in 2003. By 2006, 19 trees had been cut down and 5 additional trees had been cut by 2015. By 2015, 1 tree had been recruited and 1 tree had died, bringing the number of trees surveyed to 48. In the OTD survey, DBH was recorded for 9 trees in 2008, and 3 trees died during the period. By 2020, even more shrubs had died, so the number of trees to 39. The total BA of the trees surveyed by GDF increased in 2006 after thinning, suggesting that the impact of thinning was not negative (Fig. 5.4.2r). On the other hand, the increase in BA had leaved off since 2009 and decrease in 2020. The annual increase in DBH of individual trees appears to have declined in 2008, but has recently increased slightly (Fig. 5.4.2p, q). In fact, the average DBH increase rate was relatively large compared with other sites (Fig. 5.4.1).

(6) Dabagou (CNS007)
Dabagou (Jiwozi), located in an inland area of China, was selected as a remote site. It is a young coniferous plantation consisting mainly of two species: the evergreen *Pinus armandi* and the deciduous *Larix gmelinii*. The plantation is composed of approximately 14 tree species. At this site, DBH data from 2003 to 2024 were analyzed for GDF and OTD. The target trees of GDF were 67 in 2003. By 2016, no new trees had been recruited and 1 tree had died, leaving 66 trees for the survey. In the OTD survey, DBH was recorded for 20 *P. armandi* trees in 2008 and no dead trees were recorded during the period. However, the increase in DBH over the last 5 years was small (Fig. 5.4.2s, t). In addition, the average DBH increase rate was small (Fig. 5.4.1). This was presumed to be due to the interaction between individuals caused by high tree density. On the other hand, the total BA of the trees surveyed by GDF increased during the monitoring period (Fig. 5.4.2u). This result is considered to reflect the difference in stand characteristics between the GDF and OTD surveys.

(7) Xiaoping (CNS009)
Xiaoping, located near the sea in southern China, was selected as a remote site. The monitored stand is an evergreen broad-leaved tree plantation consisting of *Michelia macclurei* and consists of several other minor species. At this site, DBH data from 2003 to 2012 were recorded for GDF. However, individual IDs were not consistently assigned in GDF surveys, so the GDF results could not be analyzed. Therefore, only OTD data from 2008 to 2024 were analyzed. In the OTD survey, DBH was recorded for 20 *M. macclurei* trees in 2008 and 2 trees had died by 2011, reducing the number of surveyed trees to 18. The characteristics of this site is that there was almost no increase in DBH in any of the target trees during the observation period. The average DBH increase rate is very small (Figs. 5.4.1, 5.4.2v, w). However, there has been a slow but increasing trend in the long term. *M. macclurei* is not a fast-growing tree species by nature, but the cause of such extremely low growth rates is unknown.

5.4.3 Trend analysis for each stand

Tree growth is influenced by various environmental factors. These include meteorological conditions (temperature, precipitation, strong winds, and snowfall), CO_2 concentration, atmospheric depositions, intra- and inter- specific competition, diseases and pests, and anthropogenic physical disturbance, etc. (Forzieri et al. 2021; Hisano et al. 2020). The load of acid deposition (air pollution) is one such factor. Assessing the effects of air pollution through field monitoring requires appropriate monitoring plans to distinguish the effects of air pollution from other factors. As a result of air pollution control measures in China, the amount of wet deposition of nss-SO_4^{2-}, an indicator of the intensity of regional air pollution, has decreased at each survey site since 2007 (Fig. 5.3.5). In fact, the impacts of transboundary air pollution from China on the Japanese archipelago have decreased significantly since 2008 (Okamoto et al. 2018).

Sekido-san and Horyu-zan are vulnerable to air pollution from the continent, and *Fagus crenata* is a sensitive tree species to ozone stress (Kume et al. 2020). Therefore, a decrease in transboundary air pollution might have caused a systematic change in forest dynamics. At Sekido-san, the rate of DBH increase was large around 2010 to 2015, and at Horyu-zan, the rate increased around 2005 to 2010. Furthermore, stand BA increased at both sites from 2010 to 2015 (Figures 5.4.2a, b, c, d, e, f). This coincides with the expected period of decreased air pollution stress and is consistent with the results of Kume et al. (2020). Climate change has also been confirmed to have an impact on forest dynamics in this region (Ishida et al. 2026). Although no trend was observed in soil pH (Fig. 5.3.5a), the results support the idea that the forest at these sites are changing.

Ijira and Yamato are monoculture conifer plantations located inland. The effects of forest age and deforestation—that is, the interactions between trees and human disturbance—are considered significant. In particular, increased interactions among individuals as they grow are likely to have a strong effect. Under these circumstances, it is difficult to assess the effects of air pollution in isolation. However, since these two sites exhibit different density effects (Fig. 5.4.2g, h, i, j, k, l), they may serve as test sites if other factors change.

The effects of atmospheric environmental changes have been shown to vary with stand species diversity (Hisano et al. 2020). In the case of forest monitoring on Mt. Tateyama in the central mountainous region of Japan, the effects of transboundary air pollution on deciduous beech *Fagus crenata* and evergreen conifer *Cryptomeria japonica* differed, with beech becoming dominant as air pollution decreased (Kume et al. 2020). On the other hand, climate warming has had a significant impact on vegetation distribution, leading to the rise of vegetation zones (Ishida et al. 2026).

During the monitoring period, logging and thinning were the factors that most affected stand biomass at the monitoring site, and the effects of typhoons were also identified. Another factor was competition with neighboring trees, which is an aspect of biological interactions. Additionally, the study sites in China are regenerative forests and appear to be influenced by initial planting conditions. At the Dabagou GDF site, evergreen pine and deciduous larch grow together (Figure 5.4.2u), suggesting that these two tree species may have different environmental responses. From 2003 to 2012, the DBH of pine and larch increased similarly; however, after 2012, pine's rate of increase became constant, while larch's continued to increase. These results may indicate that differences in species characteristics influence interspecies relationships. However, further analysis using additional data is needed to clarify the cause.

Therefore, in order to quantitatively assess the effects of air pollution in a wide range of forests, it is necessary to identify individual trees and measure their long-term growth at sites adjacent to air quality monitoring sites with little or controlled human disturbance. It is desirable that monitoring activities be resumed and reinvigorated in countries other than Japan and China. In t future, continuous accumulation of monitoring data is expected at sites in China (Zhuxiandong, CNS011) and the Philippines (Mt. Makiling and UP Quezon, Land Grant, PHS002,102). Steady monitoring at many small-scale sites may be more effective than surveys at a few large-scale sites. In the case of planted forests, more sensitive monitoring sites may be established by adjusting the species

composition. Expanding and continuing monitoring will make it possible to assess the impact on ecosystems, including air pollution.

5.4.4 Summary

EANET conducts forest vegetation monitoring at 29 sites in 9 countries. Vegetation monitoring includes comprehensive forest surveys, tree decline surveys, and understory surveys, and the content and frequency of surveys vary widely. However, since 2015, only 8 sites in China and Japan have been surveyed more than once, and it is desirable to develop monitoring systems at each site. Wet deposition of nss-SO_4^{2-}, an indicator of regional air pollution intensity, has decreased at each survey site since 2007. However, there was no corresponding significant increase in forest growth. Most of the changes can be attributed to human disturbance, climate fluctuation, or increased competition among individuals as forest age increases. In order to quantitatively assess the effects of air pollution on a broad range of forests, it is necessary to continue to identify individual trees and measure their growth over time by monitoring air quality with little anthropogenic disturbance.

5.5 Inland water chemistry

5.5.1 Characteristics of average water chemistry for the whole monitoring

In this section, data on the inland aquatic environment collected at 17 sites in 9 countries (Table 5.5.1) were analyzed. Since the publication of the previous report (PRSAD4) five years ago, monitoring has ended at three sites, while monitoring at the Baru River in Malaysia has started. Sites lacking reported sampling data for the period from 1 January 2020 to 31 December 2024 were excluded from all tables and analysis presented in this report. Data from the starting year of each site up to 2024 were used in the analysis.

General properties of monitoring sites are important for interpreting and evaluating the monitored chemical properties of inland waters. Some properties, such as lake area, water depth, water volume, altitude and precipitation, showed large variations among sites in PRSAD3, although many data were missing. After ten years, the available information is still insufficient. The latest Data Report 2024 indicates that watershed area data are available for only 8 of the 17 sites. Information on surface geology and vegetation, which are also essential for interpreting water quality, is available only for six sites in Japan, Mongolia, Russia and Thailand (Data Report 2024).

To illustrate the characteristics of average water chemistry at each site, the relative proportions of major ions are shown in the tri-linear diagram in Figure 5.5.1, and the mean concentrations of ionic elements are compared in Figure 5.5.2. Trilinear diagrams were generated using the Python package WQChartPy (jyangfsu/WQChartPy). In each figure, panel (a) shows the total means for the period 2020–2024, while panel (b), reproduced from the previous report, represents the monitoring period from the start of monitoring to 2019.

Table 5.5.1. List of inland aquatic environment monitoring sites

Country	Site name	Site ID	Distance from the Nearest Deposition Site	Nearest Deposition Monitoring Site (Site classification)
China	Jinyunshan Lake	C1		Jinyunshan (Rural)
	Xiaoping Dam	C2		Xiaoping (Remote)
	Jiwozi River	C3		Jiwozi (Remote)
	Zhuxiandong Stream	C4		Zhuxiandong (Urban)
Japan	Ijira Lake	J1	1.1 km	Ijira (Rural)
	Futago-ike Lake Oike	J3-1	82 km	Happo (Remote)
	Futago-ike Lake Meike	J3-2	82 km	Happo (Remote)
Lao PDR	Nam Houm Lake	L1		Vientiane (Urban)
Malaysia	Baru river	Ma3		Danum Valley (Remote)
Mongolia	Terelj River	Mo1		Tereji (Remote)
Philippines	Pandin Lake	P1		Los Banos (Rural)
	Ambulalakaw Lake	P2		Mt. Sto.Tomas (Remote)
Russia	Pereemnaya River	R1	48 km	Listvyanka (Rural)
	Komarovka River	R2	0.5 km	Primorskaya (Rural)
Thailand	Vachiralongkorn Dam1 Ban Pong Chang	T1-1		Khanchanaburi (Remote)
	Vachiralongkorn Dam2 Ban Pang Pueng	T1-2		Kanchanaburi (Remote)
Vietnam	Hoa Binh Reservoir	V1		Hoa Binh (Rural)

(a)

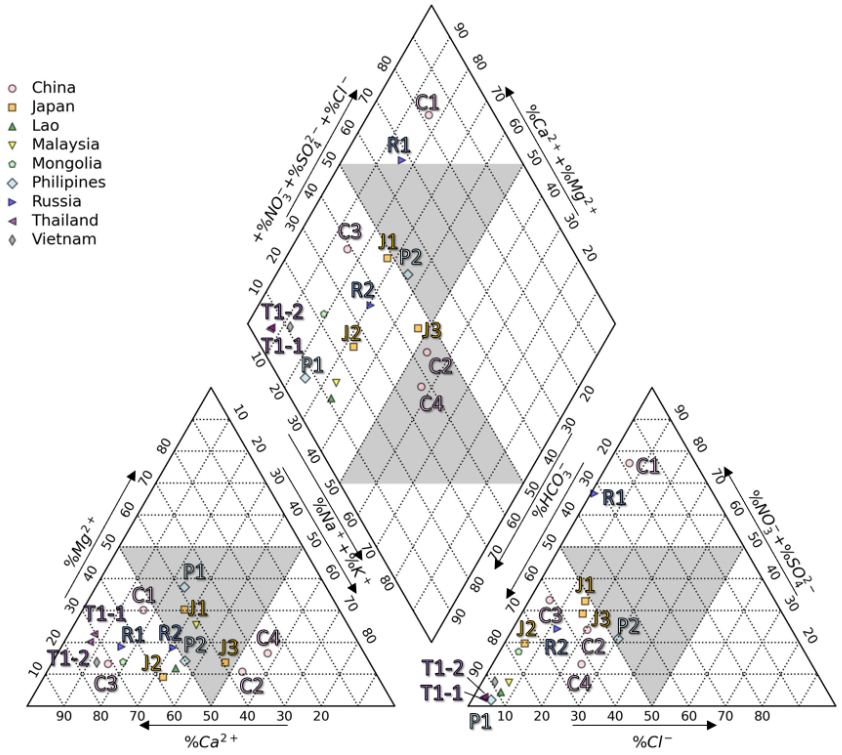

(b)

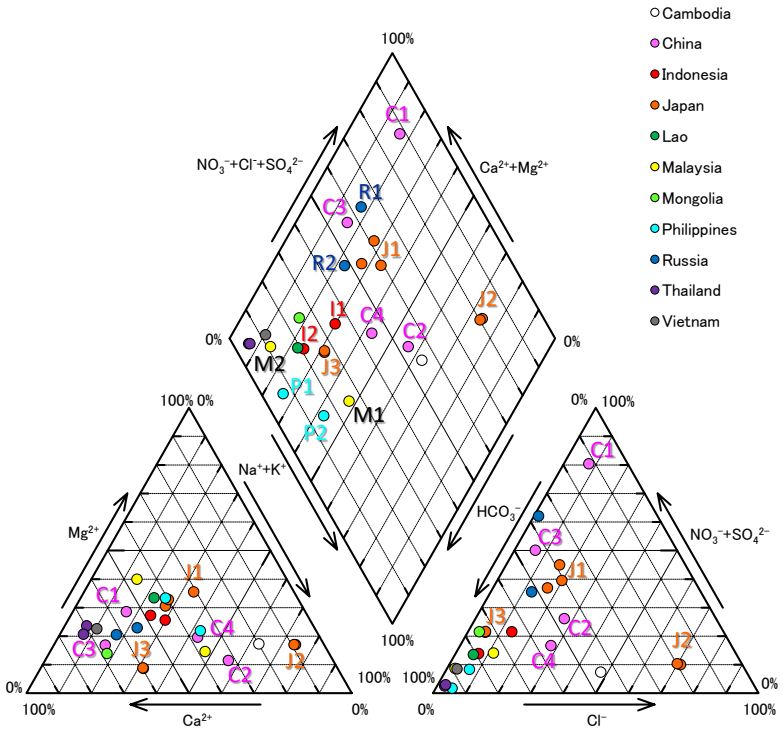

Figure 5.5.1. Piper trilinear diagram of inland water chemistry at the EANET sites. The total means for the period 2020–2024 (a) were used for plotting. Panel (b) was reproduced from the previous report and represents the monitoring period from the start of monitoring (which differs among sites) to 2019. HCO_3^- was calculated based on alkalinity. Site IDs are listed in Table 5.5.1.

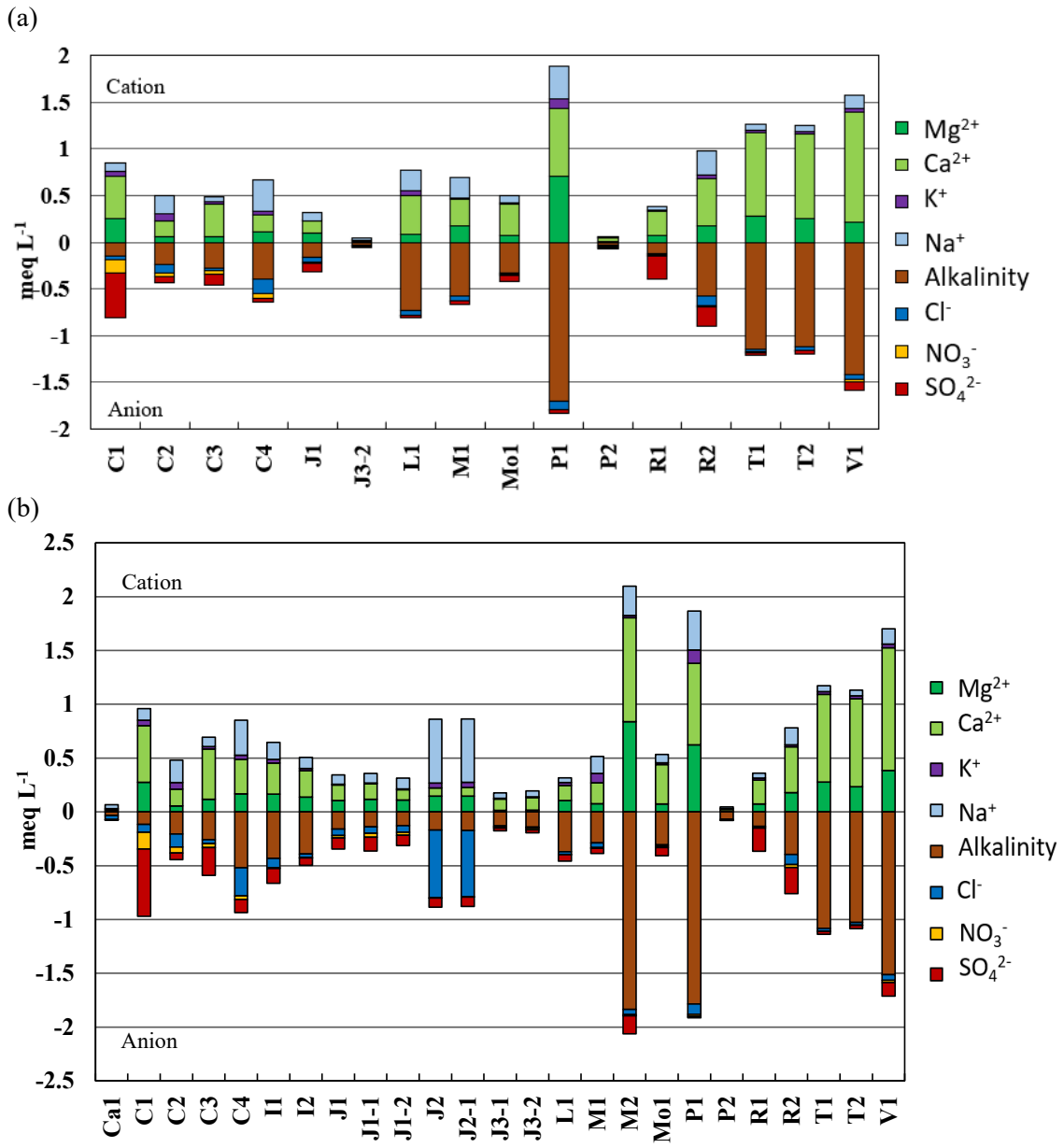

Figure 5.5.2. Mean concentrations of ionic elements in inland water at each site. The total means for the period 2020–2024 (a) were used for plotting. Panel (b) was reproduced from the previous report and represents the monitoring period from the start of monitoring (which differs among sites) to 2019.

The tri-linear diagram (Piper diagram) is commonly used to characterize inland water chemistry by showing the balance among major ions. The central diamond plot represents the balance between anions and cations, while the two triangular plots show the relative proportions of cations and anions. Although nitrate is not usually included in tri-linear diagrams, it was included in this study to examine its influence on water chemistry. The diamond field was divided by the 50% lines into four regions representing HCO_3^-–(Ca^{2+} + Mg^{2+}), HCO_3^-–(Na^+ + K^+), non-carbonate–(Ca^{2+} + Mg^{2+}), and non-carbonate–(Na^+ + K^+) water types. Here, non-carbonate anions (Cl^-, NO_3^-, and SO_4^{2-}) are collectively referred to as "non-carbonate".

While the tri-linear diagram (Figure 5.5.1) illustrates the relative proportions, the stacked concentration bars (Figure 5.5.2) highlight absolute concentrations, which are important for evaluating the sensitivity of inland waters to acidification. In particular, sites with low alkalinity (< 0.05 meq/L) may have limited buffering capacity and should be carefully monitored for potential acidification. Acid neutralizing capacity (ANC) represents the ability of water to neutralize strong acid inputs and is widely used as an indicator of the sensitivity of surface waters to acidification. Threshold values of ANC, such as 50 or 100 μeq/L, have often been used in previous studies to indicate increased vulnerability to acidification (Driscoll et al., 1993; 2001). In circumneutral waters, base cations are approximately balanced by the sum of alkalinity and strong acid anions; therefore, ANC can be approximated by alkalinity in the present study.

The tri-linear diagram and the stacked concentration bars based on data up to 2019 (Fig. 5.5.1b and Figure 5.5.2b) shows several characteristic types of ionic composition at the monitoring sites. These include waters rich in SO_4^{2-} and $Ca^{2+} + Mg^{2+}$ (C1, C3, R1, R2, and J1), waters influenced by sea salt with high proportions of Cl^- and Na^+ (J2), and waters characterized by high proportions of HCO_3^- and $Ca^{2+} + Mg^{2+}$ (P1, T1, V1, and M2).

The tri-linear diagram based on the data for 2020–2024 (Fig. 5.5.1a) generally shows patterns similar to those observed up to 2019. However, the site with sea-salt–influenced composition (J2) and one of the sites belonging to the HCO_3^-–($Ca^{2+} + Mg^{2+}$) type (M2) were not included in the recent monitoring dataset. In addition, the following changes in ionic composition were observed at several sites during 2020–2024:

1) The composition at sites C3, J1 and R2, which were categorized as non-carbonate–($Ca^{2+} + Mg^{2+}$) type in the previous report (Fig. 5.5.1b), shifted toward HCO_3^-–($Ca^{2+} + Mg^{2+}$) type (Fig. 5.5.1a).

2) The composition at site P2, which was previously classified as HCO_3^-–($Ca^{2+} + Mg^{2+}$) type (Fig. 5.5.1b), shifted toward non-carbonate–($Ca^{2+} + Mg^{2+}$) type (Fig. 5.5.1a). However, this apparent shift should be interpreted with caution because the ionic strength at site P2 is very low, as indicated by the extremely low concentrations of major ions shown in Fig. 5.5.2a. Slight changes in ionic concentrations may therefore result in large changes in relative proportions. In particular, alkalinity is as low as 0.03 meq/L, and the combined concentration of $Ca^{2+} + Mg^{2+}$ is also only 0.03 meq/L (Fig. 5.5.2a).

3) The composition at site C4, which was previously classified as HCO_3^-–($Ca^{2+} + Mg^{2+}$) type (Fig. 5.5.1b), shifted toward HCO_3^-–($Na^+ + K^+$) type (Fig. 5.5.1a).

The stacked concentration bars based on the data for 2020–2024 (Figure 5.5.2a) generally show patterns similar to those observed up to 2019 when comparisons are limited to the sites common to both periods, as several sites were not included in the recent monitoring dataset.

Based on five-year mean equivalent concentrations at each site, calcium was the most abundant cation at 15 sites, whereas sodium was the most abundant at 2 sites. Similarly, among anions, alkalinity was dominant at 15 sites, while sulfate was dominant at 2 sites.
Sites J3-2 and P2, where the mean alkalinity was below 0.05 meq/L, fall below the threshold values often used in previous studies (Driscoll et al., 1993; 2001) and therefore require particular attention with respect to potential acidification. Sites C1, J1, J3-1, and R1, where the mean alkalinity ranged from 0.10 to 0.20 meq/L, are above these thresholds but still relatively low and should also be monitored carefully for future changes.

5.5.2 Spatial patterns in inland water chemistry

Spatial patterns of inland water chemistry at the EANET monitoring sites are illustrated by the five-year mean concentrations shown on the map (Figure 5.5.3). An overview of Figure 5.5.3 shows that none of the panels exhibit a clear directional gradient in color, suggesting that the influence of transboundary air pollution is not clearly reflected in the inland water chemistry across the region.

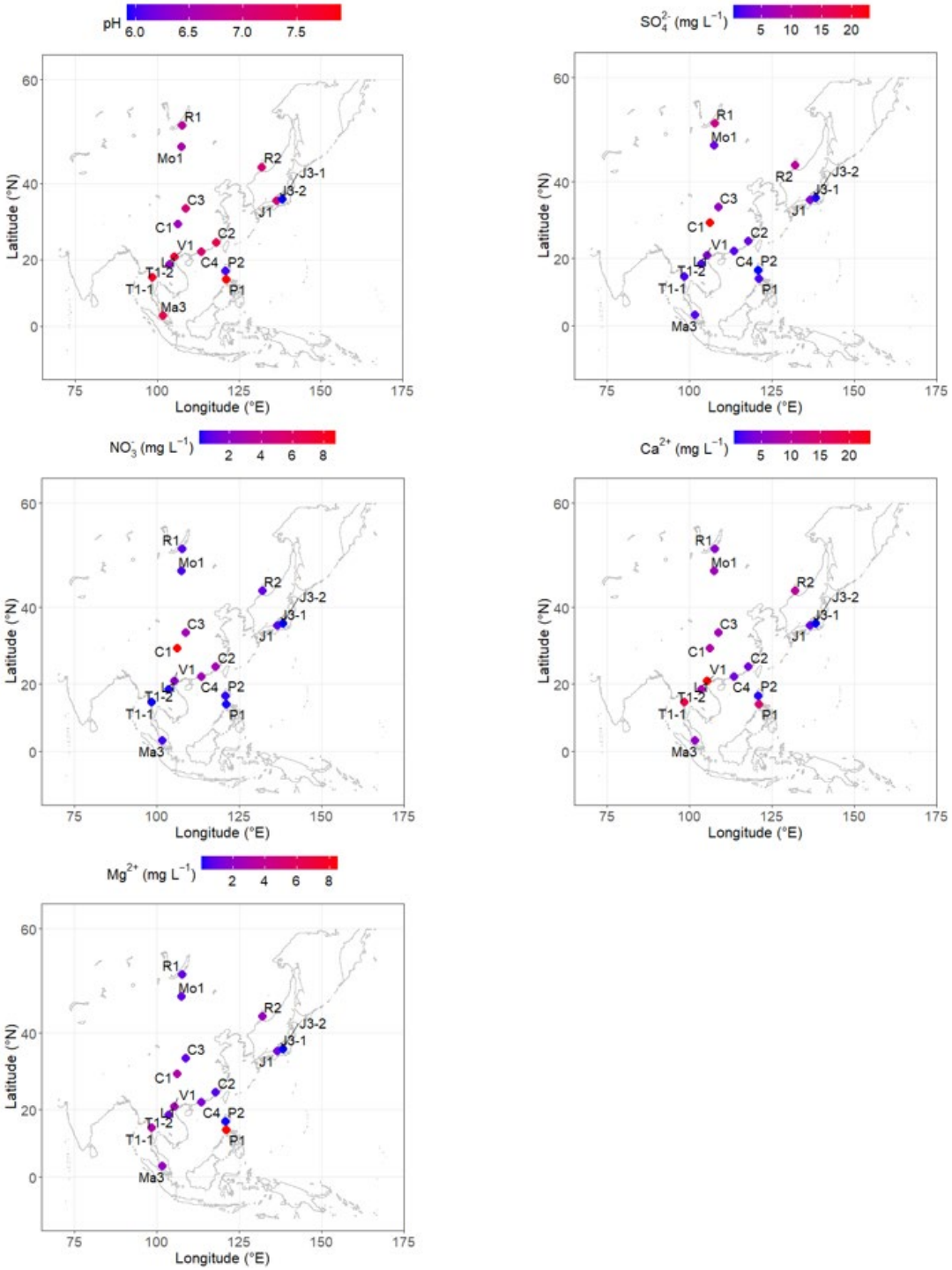

Figure 5.5.3. Spatial variability of pH values and concentrations of SO_4^{2-}, NO_3^-, Ca^{2+} and Mg^{2+} at 17 EANET inland sites. Note: values are the means from 2020 to 2024.

The mean pH ranged from 7.0 to 7.9 at 11 sites, indicating circumneutral inland waters. Among the four sites with pH values of 6.4–6.8, alkalinity was high at L1 and moderate at Mo1, whereas it was relatively low at C1 and R1, suggesting the need for careful monitoring of future changes. At the

two sites with pH values of 5.9–6.0, alkalinity was also low (0.03 meq L^{-1}), indicating a need for particular attention.

SO_4^{2-} concentrations were notably high at C1, R1, and R2, but were not as high at nearby sites such as Mo1 and C3, indicating site-to-site variability without a systematic large-scale gradient (e.g., west–east). NO_3^- concentrations were high at C1, C2, C3, C4, and V1, showing relatively elevated levels within a clustered region. Notably, at J3-2 and P2, where pH was particularly low, both sulfate and nitrate concentrations were low.

Ca^{2+} concentrations were high at V1, T1-1, T1-2, P1, R2, and C1, but were low at nearby sites such as C4, C2, and P2. At J3-2 and P2, where pH was particularly low, both Ca^{2+} and Mg^{2+} concentrations were among the lowest. Mg^{2+} concentrations showed a similar pattern to Ca^{2+}.

An overview of water chemistry across the region indicates that no sites showed the typical effects of acid deposition, characterized by high sulfate and nitrate concentrations accompanied by low calcium and magnesium concentrations leading to decreased pH. Instead, sites where low pH or high SO_4^{2-} or NO_3^- were observed are likely to have been strongly influenced by local factors such as geology and local sources.

5.5.3 Long-term patterns in inland water chemistry

Long-term patterns in inland water chemistry at the EANET monitoring sites are evaluated using the results of seasonal Mann–Kendall trend analysis (Table 5.5.2). Significance level was indicated by color: blueish color indicates increasing trend and pinkish color is decreasing trend. Z scores calculated based on the data from start year to 2024 were compared with those to 2019. Similar analysis was presented in PRSAD3, where results based on data up to 2014 were compared with those up to 2009. In PRSAD4, piecewise regression analyses were conducted for selected sites (C1 and J1) to further examine temporal changes. In addition, data provided in Data Report 2024 were also used in this section.

Jinyunshan Lake (C1)
Alkalinity increased and NH_4^+ decreased in both analyses up to 2019 and 2024. In the analysis up to 2024, SO_4^{2-}, Cl^-, and Na^+ decreased. In the analysis up to 2014, pH and alkalinity decreased, while SO_4^{2-}, NO_3^-, K^+, Ca^{2+}, and Mg^{2+} increased (PRSAD 3). However, around 2010, pH began to increase and SO_4^{2-}, NO_3^-, Ca^{2+}, and Mg^{2+} showed decreasing trends, as noted in PRSAD4. After 2019, the decreasing trend in SO_4^{2-} continued, while pH, NO_3^-, Ca^{2+}, and Mg^{2+} remained around their 2019 levels.

Xiaoping Dam (C2)
Alkalinity, K^+ and Ca^{2+} increased and Cl^- decreased in both analyses up to 2019 and 2024. In the analysis up to 2024, pH increased and NH_4^+ decreased. In the analysis up to 2014, SO_4^{2-} and K^+ increased, while NH_4^+ and Na^+ decreased (PRSAD3). At this site, an increase in K^+ and a decrease in NH_4^+ have been observed since the start of monitoring, while pH and alkalinity have increased in recent years.

Jiwozi River (C3)
Alkalinity increased and SO_4^{2-} and Ca^{2+} decreased in both analyses up to 2019 and 2024. In the analysis up to 2024, Cl^-, Na^+, and Mg^{2+} decreased. In the analysis up to 2014, pH and Na^+ decreased, while alkalinity, SO_4^{2-}, and K^+ increased (PRSAD3). At this site, an increase in alkalinity has been observed since the start of monitoring, while SO_4^{2-}, Cl^-, Na^+, Ca^{2+}, and Mg^2 have decreased in recent years.

Table 5.5.2. Results of seasonal Mann–Kendall trend analysis for inland water of the EANET sites for the data until 2019 and until 2024.

Site name		Duration		pH	EC	Alkalinity	SO_4^{2-}	NO_3^-	Cl^-	NH_4^+	Na^+	K^+	Ca^{2+}	Mg^{2+}
Jinyunshan Lake	C1	2001-	2019	-0.70	2.22	4.17	0.40	2.63	-1.20	-2.64	0.06	1.32	3.16	-0.21
			2024	0.40	-0.73	4.79	-3.02	1.22	-4.32	-2.95	-2.44	0.72	0.01	-1.85
Xiaoping Dam	C2	2001-	2019	0.08	0.67	5.14	0.86	-0.71	-2.23	-0.82	-2.80	3.22	5.65	0.00
			2024	3.37	1.33	5.23	-0.44	-1.56	-2.72	-2.16	-1.70	4.10	5.70	-0.56
Jiwozi River	C3	2001-	2019	-1.69	-1.03	6.68	-2.30	0.61	-1.92	1.56	-0.68	1.55	-2.31	-0.38
			2024	-1.40	-4.63	6.01	-6.10	1.41	-3.35	2.17	-2.61	-1.09	-4.86	-3.61
Zhuxiandong Stream	C4	2004-	2019	-3.09	2.62	2.92	-5.45	4.17	-3.74	-3.42	0.52	0.71	0.21	1.58
			2024	-2.15	0.13	0.75	-7.35	4.74	-2.36	-5.97	2.11	0.35	-2.40	-0.96
Ijira Lake	J1	2000-	2019	1.51	-5.02	0.22	-1.98	-6.32	-7.05	-6.22	-5.28	-3.38	-4.11	-5.26
			2024	1.53	-6.42	0.80	-3.78	-8.14	-8.61	-6.78	-6.11	-3.76	-4.24	-6.33
Futago Lake oike	J3-1	2019-	2019											
			2024	0.83	1.10	2.01	-3.22	1.64	1.61		2.08	0.04	0.68	1.10
Futago Lake meike	J3-2	2019-	2019											
			2024	-1.21	-3.22	-0.73	-4.63	-2.05	0.646		0.833	-2.52	-2.62	-3.43
Nam Houm Lake	L1	2009-	2019	1.06	-1.33	-1.91	2.04	-1.66	-2.58					
			2024	-1.10	1.10	0.57	0.00	-0.93	-0.34	0.00	2.33	0.00	0.36	-0.54
Baru river	Ma3	2022-	2019											
			2024	-1.44	-2.92	-3.45	-2.62	1.71	1.25	2.16	-0.19	-2.62	-3.75	-3.30
Terelj river	Mo1	2002-	2019	-2.87	0.02	1.42	4.43	-1.46	-1.89	0.60	-1.50	-0.64	-1.00	-1.96
			2024	-4.05	-2.28	2.20	2.07	-3.28	-1.34	2.13	-1.03	0.15	-0.33	-1.93
Pandin Lake	P1	2004-	2019	-0.29	0.66	0.09	3.27	-1.72	0.46	0.05	0.74	-3.64	3.68	-0.28
			2024	0.91	0.69	-0.08	6.77	-3.81	0.43	-1.08	1.26	-3.46	2.08	2.03
Ambulalakaw Lake	P2	2005-	2019	1.01	1.17	-0.82	-2.05	-1.80	-0.02	-0.32	2.55	1.00	-0.12	0.91
			2024	1.90	4.59	-1.22	-2.23	-2.13	1.63	-0.77	-0.57	0.38	0.37	0.33
Pereemnaya River	R1	2004-	2019	-0.09	1.74	-1.64	3.96	-1.49	-1.31	-5.46	0.52	-1.67	3.78	-1.76
			2024	0.38	2.41	-1.73	4.57	-1.13	-3.38	-6.59	0.50	-0.93	4.38	-1.24
Komarovka River	R2	2005-	2019	-4.60	0.47	-2.32	3.20	5.70	0.33	0.68	3.12	3.74	1.33	-1.84
			2024	-2.89	-1.23	1.29	-0.67	0.85	0.36	-0.10	6.50	7.25	3.23	-1.45
Vachiralongkorn Dam 1	T1-1	2000-	2019	0.46	0.84	2.33	0.48	1.14	2.21	2.11	3.70	1.35	3.06	2.11
			2024	0.98	2.75	2.70	0.79	1.52	4.42	2.05	4.55	1.39	4.55	2.24
Vachiralongkorn Dam2	T1-2	2000-	2019	2.66	0.43	4.49	0.91	2.49	1.78	1.71	2.47	0.34	3.46	1.11
			2024	2.62	3.33	5.33	1.43	2.95	4.24	0.79	3.52	0.83	5.09	2.80
Hoa Binh Reservoir	V1	2000-	2019	-0.31	-1.49	-4.14	-0.04	3.66	2.49	-4.17	3.14	0.75	-2.48	-2.15
			2024	-0.50	-2.63	-4.96	-2.79	5.02	1.77	-1.47	2.48	3.55	-1.17	-6.14

$p < 0.05$	-	+
$p < 0.01$	-	+
$p < 0.001$	-	+

Note : Value shows Z score, which indicates the increasing trend with positive values or the decreasing trend with negative values. Color shows significant levels.

Zhuxiandong Stream (C4)

NO_3^- increased and pH, SO_4^{2-}, Cl^- and NH_4^+ decreased in both analyses up to 2019 and 2024. In the analysis up to 2024, Na^+ increased and Ca^{2+} decreased. In the analysis up to 2014, Cl^- and Na^+ decreased, while alkalinity increased (PRSAD3). At this site, a decrease in Cl^- has been observed since the start of monitoring, while pH has decreased and NO_3^- has increased in recent years.

Ijira Lake (J1)

SO_4^{2-}, NO_3^-, Cl^-, NH_4^+, Na^+, K^+, Ca^{2+}, and Mg^{2+} decreased in both analyses up to 2019 and 2024. In the analysis up to 2014, NO_3^-, Cl^-, NH_4^+, Na^+, K^+, Ca^{2+}, and Mg^{2+} decreased, while pH increased (PRSAD3). In PRSAD4, an increasing trend in Ca from 2016 to 2019 was noted; however, after 2020, a decreasing trend has continued. At this site, a decrease in NO_3^-, Cl^-, NH_4^+, Na^+, K^+, Ca^{2+}, and Mg^{2+} has been observed since the start of monitoring, while SO_4^{2-} has also decreased in recent years.

Futago-ike Lake Oike (J3-1)

At this site, where monitoring began in 2019, increasing trends in alkalinity and Na^+ and a decreasing trend in SO_4^{2-} were observed up to 2024.

Futago-ike Lake Meike (J3-2)
At this site, where monitoring began in 2019, decreasing trends in SO_4^{2-}, NO_3^-, K^+, Ca^{2+}, and Mg^{2+} were observed up to 2024.

Nam Houm Lake (L1)
This site was monitored in 2009, 2014, from 2016 to 2019, and in 2024. In the analysis up to 2019, an increasing trend in SO_4^{2-} and a decreasing trend in Cl^- were observed, whereas in the analysis up to 2024, only an increasing trend in Na^+ was observed.

Baru River (Ma3)
At this site, where monitoring began in 2022, decreasing trends in alkalinity, SO_4^{2-}, K^+, Ca^{2+}, and Mg^{2+}, and a increasing trend in NH_4^+ were observed up to 2024.

Terelj River (Mo1)
SO_4^{2-} increased and pH decreased in both analyses up to 2019 and 2024. In the analysis up to 2024, alkalinity increased and NO_3^- decreased. In the analysis up to 2014, alkalinity and SO_4^{2-} increased, while NO_3^- decreased (PRSAD3). At this site, a decrease in NO_3^- and an increase in alkalinity and SO_4^{2-} have been observed since the start of monitoring, while pH has decreased in recent years.

Pandin Lake (P1)
SO_4^{2-} and Ca^{2+} increased and K^+ decreased in both analyses up to 2019 and 2024. In the analysis up to 2024, Mg^{2+} increased and NO_3^- decreased. In the analysis up to 2014, Ca^{2+} increased, while K^+ decreased (PRSAD3). At this site, a decrease in K^+ and an increase in Ca^{2+} have been observed since the start of monitoring, while SO_4^{2-} and Mg^{2+} have increased and NO_3^- has decreased in recent years.

Ambulalakaw Lake (P2)
This site was monitored in 2005, from 2007 to 2009, from 2013 to 2016, and from 2022 to 2024. SO_4^{2-} decreased in both analyses up to 2019 and 2024. In the analysis up to 2024, NO_3^- decreased. In the analysis up to 2014, NH_4^+ increased, while NO_3^- decreased (PRSAD3). At this site, a decrease in NO_3^- has been observed since the start of monitoring, while SO_4^{2-} has decreased in recent years.

Pereemnaya River (R1)
SO_4^{2-} increased and NH_4^+ decreased in both analyses up to 2019 and 2024. In the analysis up to 2024, Cl^- decreased. In the analysis up to 2014, SO_4^{2-} and Ca^{2+} increased, while NO_3^-, NH_4^+, and Mg^{2+} decreased (PRSAD3). At this site, an increase in SO_4^{2-} has been observed since the start of monitoring.

Komarovka River (R2)
Na^+ and K^+ increased and pH decreased in both analyses up to 2019 and 2024. In the analysis up to 2024, Ca^{2+} decreased. In the analysis up to 2014, pH and alkalinity decreased, while NO_3^- and NH_4^+ increased (PRSAD3). At this site, a decrease in pH has been observed since the start of monitoring, with considerable variability in the data.

Vachiralongkorn Dam1 (Ban Pong Chang) (T1-1)
Alkalinity, Cl^-, NH_4^+, Na^+, Ca^{2+}, and Mg^{2+} increased in both analyses up to 2019 and 2024. In the analysis up to 2014, Cl^- decreased. At this site, NH_4^+, Na^+, Ca^{2+}, and Mg^{2+} have increased in recent years.

Vachiralongkorn Dam2 (Ban Pang Pueng) (T1-2)
pH, alkalinity, NO_3^-, Na^+, and Ca^{2+} increased in both analyses up to 2019 and 2024. In the analysis up to 2024, Cl^- and Mg^{2+} increased. In the analysis up to 2014, alkalinity increased, while Cl^- decreased (PRSAD3). At this site, an increase in alkalinity has been observed since the start of monitoring, while pH, NO_3^-, Cl^-, Na^+, Ca^{2+}, and Mg^{2+} have increased in recent years.

Hoa Binh Reservoir (V1)
Alkalinity and Mg^{2+} decreased, and NO_3^- and Na^+ increased in both analyses up to 2019 and 2024. In the analysis up to 2024, SO_4^{2-} decreased, while K^+ increased. In the analysis up to 2014, alkalinity, NH_4^+, and Mg^{2+} decreased, while NO_3^-, Cl^-, and Na^+ increased (PRSAD3). At this site, a decrease in alkalinity and Mg^{2+} has been observed since the start of monitoring, while SO_4^{2-} has decreased and NO_3^-, Na^+, and K^+ have increased in recent years.

Focusing on pH in long-term changes, among the sites where decreasing trends in pH were observed up to 2014 in PRSAD 3 (C1, C2, C3, and R2), no such trend in pH was observed up to 2024 at three sites (C1, C2, and C3), except for R2. At the three sites (C4, Mo1, and R2) where decreasing trends in pH were observed up to 2024, no decreasing trend in alkalinity was found, and the absolute values of pH, alkalinity, and Ca concentrations were relatively high. Therefore, the risk of immediate acidification at these sites is considered to be low.

Overall, the trends at the 17 sites indicate that long-term patterns varied widely among sites, reflecting site-specific processes rather than a consistent regional pattern. Against this background, several notable changes were identified when the trend analysis based on data up to 2024 was compared with that based on data up to 2014 using the same methodology as applied in PRSAD3. In particular, some trends that were not statistically significant in PRSAD3 ($p \geq 0.01$) became highly significant in the present analysis ($p < 0.001$), as shown in Table 5.5.2.

Changes potentially related to acidification were observed at some sites. A decreasing trend in pH was found at Mo1, while increasing trends in NO_3^- concentrations were detected at C4 and V1. In contrast, changes opposite to acidification were also identified. Alkalinity increased at C1 and T1-2, and both pH and alkalinity increased at C2. In addition, decreasing trends in SO_4^{2-} concentrations were observed at C4 and J1. These findings indicate that, although site-specific processes dominate the long-term patterns, some sites have shown distinct changes in the most recent period. The relationships between these changes and atmospheric deposition are discussed in the following section.

5.5.4 Relationships with atmospheric deposition

As described in the previous section, long-term patterns in inland water chemistry varied considerably among sites. This site-specific variability suggests that the influence of atmospheric deposition may also differ among sites depending on local catchment characteristics and buffering capacity.

Previous studies have also indicated that the relationship between atmospheric deposition and inland water chemistry is not straightforward. Duan et al. (2016), reviewing studies from the 1990s to the early 2010s, reported that although atmospheric deposition of sulfur (S) and nitrogen (N) has been relatively high in many parts of East Asia, the response of inland water chemistry has generally been limited due to substantial buffering capacity and biogeochemical processes within catchments. On the other hand, long-term observations in regions where atmospheric deposition has decreased since the 1980s have shown that changes in deposition can lead to gradual recovery processes in catchments, including reductions in acid-related parameters such as aluminum mobilization and associated shifts in biogeochemical functioning (Ohte, 2025).

Against this background, this section examines the relationships between atmospheric deposition and inland water chemistry at the EANET monitoring sites, focusing on both spatial patterns and long-term trends. Total deposition data (including both wet and dry components) were used for the assessment at J1, J3, R1, R2, and V1. For the remaining sites (C1–C4, L1, Ma3, Mo1, P1, P2, and T1), wet deposition data were used instead because total deposition data were not available due to the absence of filter pack (FP) measurements, lack of recent data, or incomplete chemical coverage.

According to PRSAD4, comparisons between wet deposition and inland water chemistry across the EANET monitoring sites revealed no clear and consistent relationships in either spatial patterns or

long-term trends. Sites with relatively high deposition did not necessarily exhibit lower pH or higher concentrations of acid-related ions, and temporal changes in deposition were not always directly reflected in corresponding changes in water chemistry.

Nevertheless, some site-specific correspondences were observed. For example, at Ijira Lake (J1) in Japan, decreasing trends in the deposition of acidic components since the early 2000s were accompanied by increasing pH and decreasing concentrations of SO_4^{2-} and NO_3^-, indicating recovery from acidification. Similar recovery patterns were also suggested at several sites in China (C1–C4) and at Patenggang Lake (I1) in Indonesia (PRSAD4).

To extend the findings of PRSAD4, relationships between atmospheric deposition and inland water chemistry were further examined using long-term monitoring records available at each site. At several sites, long-term changes in inland water chemistry were not clearly associated with changes in atmospheric deposition. For example, SO_4^{2-} concentrations in inland water at L1 showed an increasing trend during 2009–2019 (Table 5.5.2), whereas no corresponding trend was observed in atmospheric deposition. At Mo1, SO_4^{2-} concentrations in inland water chemistry showed increasing trends, while NO_3^- concentrations showed decreasing trends (Table 5.5.2). In contrast, atmospheric deposition showed episodically high sulfur deposition in 2015, 2016, and 2021, and relatively high nitrogen deposition during 2002–2008 and in 2021. At T1, nitrogen-related parameters in inland water chemistry showed increasing trends (Table 5.5.2), whereas atmospheric deposition showed no clear long-term trend. At R1, total sulfur and nitrogen deposition remained generally stable during the available observation period from 2015 onward, while sulfate concentrations in inland water showed an increasing tendency and nitrate concentrations showed no clear trend (Table 5.5.2). At V1, total sulfur and nitrogen deposition fluctuated considerably during 2015–2024 without clear long-term trends, whereas sulfate concentrations in inland water showed a decreasing tendency and nitrate concentrations an increasing tendency (Table 5.5.2). These examples indicate that temporal patterns in inland water chemistry were often inconsistent with year-to-year variations in atmospheric deposition, suggesting that inland water chemistry was influenced not only by contemporary atmospheric deposition but also by other processes operating within the catchment. Responses of inland water chemistry to atmospheric deposition are likely influenced not only by current deposition inputs but also by the accumulation and retention of deposited substances within catchments. Consequently, changes in water chemistry may occur with substantial time lags and may differ among sites depending on catchment characteristics, hydrological conditions, and biogeochemical processes.

In contrast, several sites showed corresponding changes between atmospheric deposition and inland water chemistry. At C1, sulfur- and nitrogen-related parameters showed decreasing trends after around 2010 in both inland water chemistry and atmospheric deposition. At C3, sulfur-related parameters in inland water chemistry increased until around 2014 and subsequently decreased. Atmospheric sulfur deposition was also lower after 2014 than in the preceding period. At C4, sulfur-related parameters in inland water chemistry showed decreasing trends that coincided with decreasing sulfur deposition. At J1, sulfur and nitrogen deposition showed decreasing tendencies during the available observation period. SO_4^{2-}, NO_3^-, and NH_4^+ concentrations in inland water also showed decreasing trends in both the 2000–2019 and 2000–2024 analyses (Table 5.5.2), suggesting a correspondence between atmospheric deposition and inland water chemistry.

Several sites showed only partial correspondence. At C2, atmospheric deposition showed decreasing trends in sulfur and nitrogen, while inland water chemistry showed a clear increasing trend in pH (Table 5.5.2), although sulfur- and nitrogen-related parameters in inland water did not exhibit clear trends. At P1, sulfate concentrations in inland water increased during 2004–2024 despite generally stable sulfur deposition. However, cumulative sulfur deposition during 2000–2024 was relatively high (153 kg ha^{-1}), suggesting that long-term accumulation within the catchment may have contributed to the gradual increase in sulfur export.

At J3, total deposition data were available only for 2021–2022 and were therefore insufficient for evaluating long-term relationships with inland water chemistry. At Ma3, inland water monitoring started in 2022 and the site was therefore not suitable for assessment of long-term relationships. Nevertheless, both wet sulfur deposition and sulfate concentrations in inland water decreased during the available observation period, although the record is too short to evaluate the relationship in detail.

At R2, trend analysis indicated increasing trends in SO_4^{2-} and NO_3^- concentrations during 2005–2019, whereas no significant trends were detected for the period 2005–2024 (Table 5.5.2). Examination of the recent data suggests that both SO_4^{2-} and NO_3^- concentrations decreased during 2019–2024, offsetting the earlier increasing tendencies. Total sulfur and nitrogen deposition, however, remained generally stable during 2015–2023. These results suggest that the recent decreases in SO_4^{2-} and NO_3^- concentrations were not clearly associated with changes in atmospheric deposition during the available observation period.

Taken together, sulfur-related changes in inland water chemistry tended to show better correspondence with atmospheric deposition than nitrogen-related changes. Nitrogen-related parameters often showed weak or inconsistent relationships with atmospheric deposition, suggesting substantial influences of internal catchment processes such as biological uptake and nitrogen transformation.

In addition, several of the sites showing clearer correspondence between atmospheric deposition and inland water chemistry were characterized by relatively high sulfur loading. The Chinese sites (C1–C4), where cumulative sulfur deposition exceeded approximately 100 kg ha^{-1} during 2000–2024, showed some of the most evident relationships. A similar pattern was observed at J1, where recovery of inland water chemistry coincided with decreasing atmospheric deposition and where historically high sulfur loading associated with industrial emissions has been reported (Sase et al., 2019). These observations imply that atmospheric deposition may be more readily reflected in inland water chemistry at sites with relatively high sulfur loading, although the influence of catchment-specific processes remains substantial. Overall, the results suggest that responses of inland water chemistry to atmospheric deposition are highly site-specific and are influenced not only by atmospheric inputs but also by catchment characteristics and biogeochemical processes.

5.5.5 Summary

Inland water chemistry at 17 EANET sites during 2020–2024 showed substantial site-to-site variability, with no clear regional pattern attributable to transboundary air pollution. Long-term trends also varied considerably among sites, indicating that changes in water chemistry do not necessarily parallel trends in atmospheric deposition. Nevertheless, recovery from acidification continued to be observed at some sites, such as Ijira Lake, where changes in water chemistry corresponded with decreasing atmospheric deposition. Such correspondence was generally more evident for sulfur-related than for nitrogen-related parameters. Overall, responses of inland water chemistry to atmospheric deposition were highly site-specific and were influenced not only by atmospheric inputs but also by catchment characteristics, hydrological conditions, and biogeochemical processes.

5.6 Catchment-scale analysis

The atmospheric environment in the East Asian region has changed substantially over the past two decades due to economic development, as well as efforts to prevent its harmful impacts on human health and terrestrial ecosystems. To assess the possible impacts of atmospheric deposition on ecosystems, monitoring of soil, forest vegetation, and inland water has been conducted, as discussed above. However, atmospheric deposition and its impacts on ecosystems are often monitored independently in different locations, and in many ecological monitoring sites they are not necessarily linked to each other for assessment. Therefore, integrated monitoring that covers the flow from atmospheric deposition to terrestrial ecosystems is required to adequately assess these impacts.

To achieve the above objective, EANET has promoted catchment-scale analysis using small forest catchments as unit areas, enabling quantitative and qualitative assessments of the relationships between atmospheric deposition and ecosystem responses. Based on case studies conducted in Japan, Malaysia, and Thailand since the early 2000s, the "*Guideline for Catchment-scale Monitoring in East Asia*" was developed by the Task Force on Soil and Vegetation Monitoring and adopted in 2010. Following this, regular catchment-scale monitoring was initiated at the Lake Ijira catchment (IJR) and the La Mesa Watershed (LMW), and monitoring data collected at IJR since 2007 were also submitted to EANET. In addition, inland water data accumulated at the Komarovka River catchment (KMR) and the Pereemnaya River catchment (PRN) have been evaluated on a catchment scale together with atmospheric deposition data collected in surrounding areas. The locations of the monitoring sites used for catchment-scale analysis and the characteristics of each catchment site are shown in Table 5.6.1 and Fig. 5.6.1, respectively.

Table 5.6.1 Characteristics of each catchment site

Site name (name of river/stream)	Catchment area (km^2)	Forest type	Soil type	Data available since
Komarovka River catchment (KMR)	155	Broadleaved forest	Umbric Cambisols, Mollic Liptosol	2005
Pereemnaya River catchment (PRN)		Boreal forest		2005
Lake Ijira catchment (IJR) (Kamagatani River)	2.98 (at Kamagatani River)	Coniferous tree plantation	Chert, Cambisols	2007
La Mesa Watershed (LMW) (stream at Tower 1 Station)	0.18 (at Tower 1 stream)	Secondary forest	Clastic and volcanic rocks, Loamy-sand soil	2019

Note. "Data available since" indicates the first year for which monitoring data were available for catchment-scale analysis.

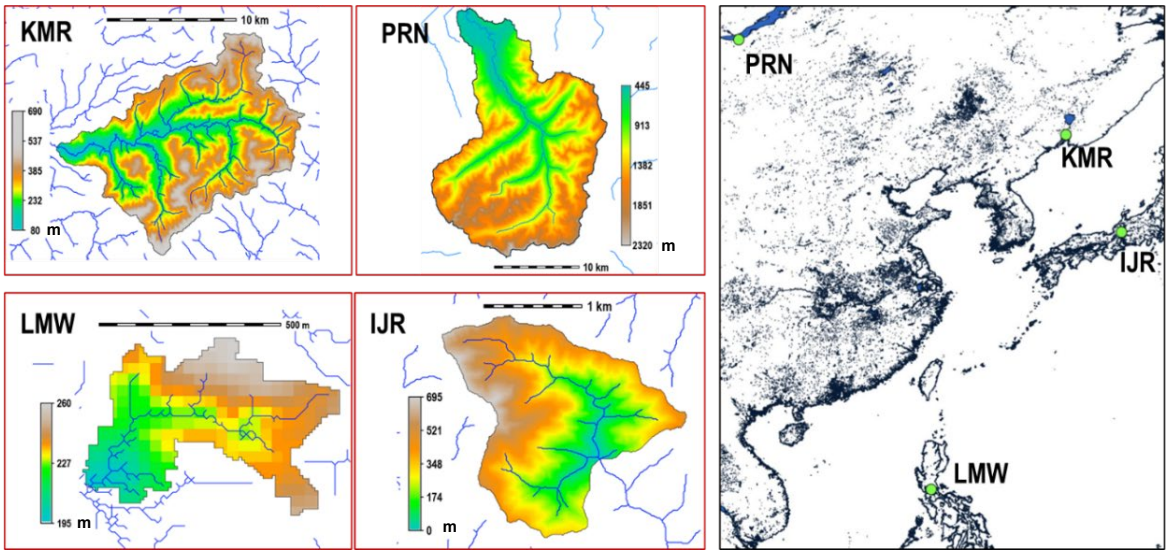

Fig. 5.6.1 Locations of the monitoring sites used for catchment-scale analysis. The vertical color scale indicates distribution of altitudes within each catchment area. KMR, Komarovka River catchment; PRN, Pereemnaya River catchment; IJR, Lake Ijira catchment; LMW, La Mesa Watershed (LMW).

5.6.1 Long-term trends of atmospheric deposition and stream water chemistry

For the monitoring sites used for catchment-scale analysis, atmospheric deposition is monitored either within the catchment area or at locations within the same region as the target forest area. Changes in stream water chemistry draining from the catchment area may therefore reflect regional variations in atmospheric deposition. Long-term trends of atmospheric deposition and stream water chemistry at the respective catchment sites are compared in Fig. 5.6.2 for sulfate (SO_4^{2-}) and dissolved inorganic nitrogen (DIN; NO_3^- + NH_4^+). In this figure, total atmospheric deposition is calculated as the sum of wet and dry deposition. Dry deposition fluxes were estimated using filter-pack air concentration data together with available meteorological data, following the methodology described in the *Technical Manual for Dry Deposition Flux Estimation in East Asia–2010* (EANET 2010).

1) KMR

Although deposition fluxes for sulfur (S) and DIN do not show any significant trends, the decreasing trends for SO_2, SO_4^{2-}, HNO_3 NH_3 and NH_4^+ concentrations in atmospheric air are observed. In the period 2019-2023 S and DIN wet deposition showed a tendency to increase; however, all changes remained within the range of interannual variability. Overall, the proportion of wet deposition in the total precipitation amount increases.

SO_4^{2-} and DIN concentrations in precipitation show no visible tendencies in last five years. pH values, which earlier showed a continuous trend to increase, appear to show a slight decline after 2020. Nevertheless, a trend toward increased precipitation persists, particularly during the warm season. This may partly account for the enhanced leaching of S and nitrogen (N) compounds in the KMR, thereby contributing to soil water acidification (Zhigacheva et al., 2022).

Prior to 2021 for SO_4^{2-} and 2017 for DIN, stream water in the KMR exhibited a significantly increasing trend in concentrations. Following these respective years, a decreasing tendency began. The decline is especially marked for SO_4^{2-}, with the decrease appearing remarkably steep.

2) PRN

For stream water, DIN shows a decreasing trend, though periodic increases have occurred in recent years. Simultaneously, a decline in NO_3^--N concentrations in precipitation has been recorded in the region during the past ten years. SO_4^{2-} in precipitation in contrast, exhibits a significant increasing concentration trend.

The current ionic composition of the Pereemnaya River water is classified as an SO_4^{2-}–Ca^{2+} water type, which had previously been observed only episodically. The water shows elevated SO_4^{2-} and NO_3^- levels, low pH (6.43–7.01), and poor buffering capacity due to rainwater feeding, making it vulnerable to acidification.

3) IJR

Total atmospheric deposition of SO_4^{2-}-S has decreased significantly over the observation period. Because IJR is located in an inland mountainous area, the non-sea-salt (nss) fraction exhibited a similar decreasing trend. Deposition of DIN has also declined, although the decrease was relatively moderate compared with that of S. Consistent with the changes in atmospheric deposition, concentrations of SO_4^{2-} and DIN (predominantly NO_3^- in the case of IJR) in stream water have decreased over the observation period, suggesting that stream water chemistry at IJR has responded sensitively to changes in atmospheric deposition.

The forest ecosystem at IJR was considered to be acidified and N-saturated in the mid-1990s due to high atmospheric deposition of acidic substances combined with climatic anomalies in 1993/1994 (Nakahara et al., 2010). As suggested by Sase et al. (2019), recovery from acidification and N saturation appears to have progressed in response to the subsequent decline in atmospheric deposition. However, DIN deposition has not decreased, and has even shown a slight increase, during the most recent five-year period. Although stream water NO_3^- concentrations have continued to

decline since 2000, continued monitoring in relation to atmospheric deposition is warranted. In addition, SO_4^{2-} concentrations in stream water were consistently much higher than those of NO_3^-. At IJR, a contribution from geological S has been reported (Sase et al., 2019), and its influence is discussed further below.

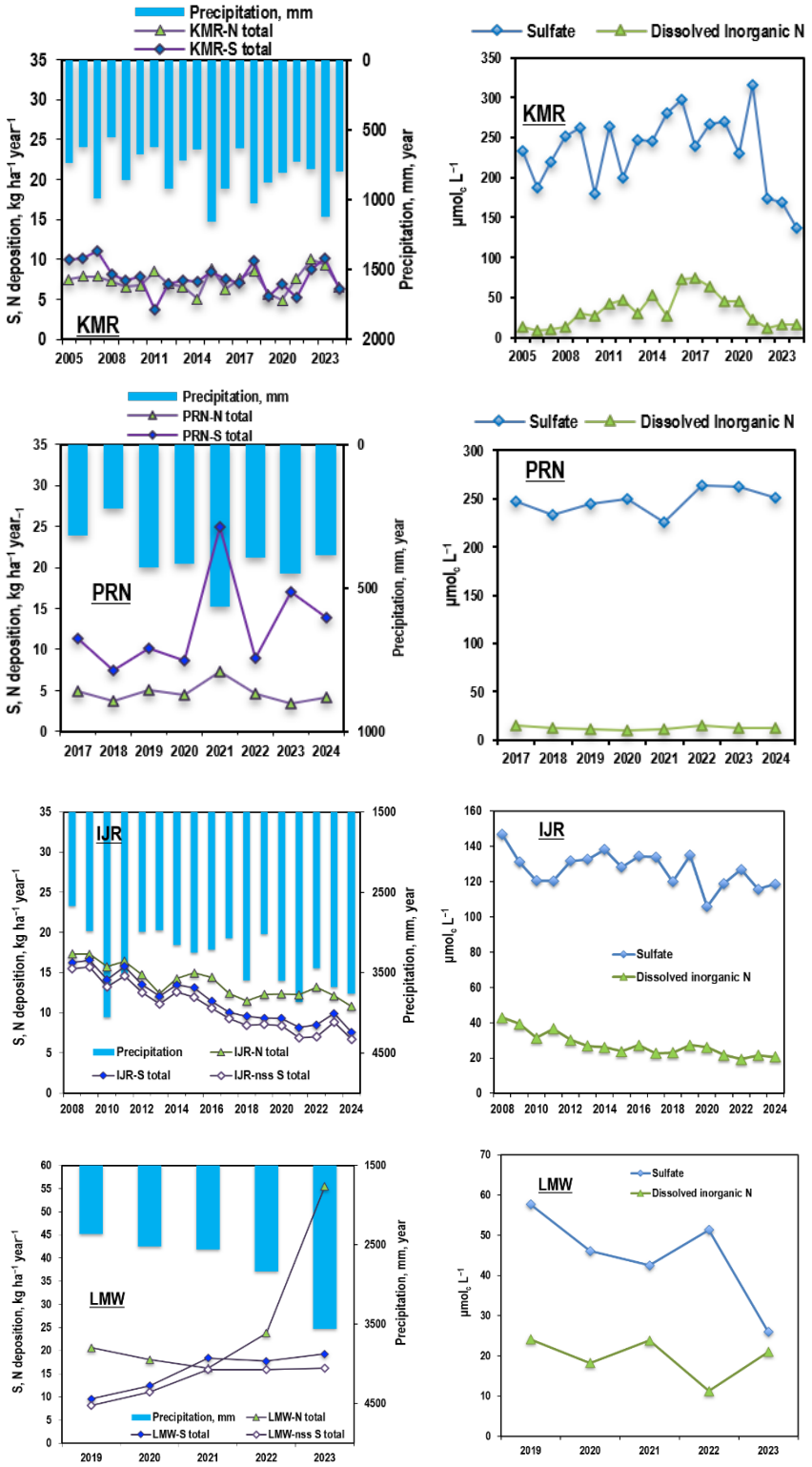

Fig. 5.6.2 Variations of total atmospheric deposition (wet and dry) and stream water concentrations of sulfur (S) and dissolved organic nitrogen (DIN) at KMR, PRN, IJR, and LMW. "nss", non-sea-salt

During the 2019–2023 observation period, atmospheric deposition at La Mesa Watershed showed increasing tendencies for both S and DIN, with the increase in DIN being more pronounced, particularly in 2023. The marked rise in DIN deposition coincided with the highest annual precipitation, suggesting the influence of enhanced wet deposition during high-rainfall conditions.

In contrast, stream water chemistry did not show a proportional increase in response to atmospheric inputs. SO_4^{2-} concentrations in stream water fluctuated during the observation period and declined sharply in 2023 despite the continued input of S deposition. This suggests that stream water SO_4^{2-} was influenced not only by atmospheric deposition but also by catchment processes such as hydrologic dilution, soil and groundwater interactions, delayed release of stored S, or possible geologic contributions.

DIN concentrations in stream water remained consistently lower than those in rainwater, even during the period of increased N deposition. This indicates substantial retention or transformation of inorganic N within the watershed, likely through biological uptake, microbial processes, and soil storage. The results suggest that La Mesa Watershed continues to function as a N-buffering system.

Overall, the observed trends indicate that stream water chemistry at La Mesa Watershed does not respond immediately or linearly to changes in atmospheric deposition. While the catchment appears to retain much of the deposited N, the recent increase in DIN deposition warrants continued monitoring, particularly of NH_3 and NH_4^+, to assess potential risks of N saturation and future changes in watershed nutrient dynamics.

5.6.2 Input-output balances in forest catchments

Material fluxes via stream water can be estimated based on solute concentrations and water discharge, in a manner similar to the estimation of atmospheric deposition. Comparing material balances between atmospheric inputs and outputs via stream water provides useful information on the sources of materials, as well as their retention and cycling within forest ecosystems. Accordingly, inputs and outputs, calculated on a unit-area basis using the catchment area, are compared in Fig. 5.6.3 for SO_4^{2-} and DIN.

1) KMR

Despite the changing trends in stream water concentrations, the relationship between input and output fluxes remains consistent with that observed in previous years. S output is more than twice as high as input, whereas the input of DIN considerably exceeds its output.

The observed S imbalance is typical for certain recovering catchments and is commonly attributed to the mobilization of previously accumulated S in catchment soils. However, S leaching may also be related to bedrock weathering or to mobilization processes enhanced by humid conditions. Given that precipitation amounts at the KMR have been increasing over recent decades, it would be premature to conclude that the KMR has commenced recovery from acidification.

2) PRN

As observed at KMR, the S input to PRN is significantly lower than its output, suggesting internal catchment release of S. The sources of this excess S export are yet to be identified.

Despite a rising trend in NO_3^- concentration in precipitation over the past decade, the total atmospheric N deposition does not show a corresponding increase; on the contrary, it tends to decrease. The stream water output largely mirrors the input pattern, though at roughly half the output flux level.

3) IJR

At IJR, S output via stream water significantly exceeded atmospheric input, suggesting the presence of S sources other than atmospheric deposition. In contrast, the output of DIN was equivalent to

nearly 70% of the atmospheric input, indicating that a substantial fraction of the deposited DIN was not retained or utilized within the forest ecosystem.

Although S is an essential element for plant growth, previous studies have reported that atmospheric inputs and outputs via stream water are generally well balanced in forest ecosystems where atmospheric deposition is the primary source of S (Sase et al., 2021; Saito et al., 2023). In contrast, at IJR, geological S has been suggested as another major S source in stream water based on S isotope ($\delta^{34}S$) analysis (Sase et al., 2019). Accordingly, baseline concentrations of SO_4^{2-} in stream water appear to be controlled largely by geological S and meteorological and hydrological conditions. Nevertheless, the observed long-term decreasing trend indicates that atmospheric S has also contributed to SO_4^{2-} concentrations in stream water at IJR.

N is an essential element for plant growth. In healthy forest ecosystems, atmospherically derived N is efficiently cycled and assimilated by vegetation, and only small amounts leach into stream water. However, excessive atmospheric N inputs can exceed ecosystem demand, leading to N saturation and disruption of biogeochemical cycles, including increased N leaching to streams (Aber et al., 1998; Stoddard, 1994). The forest ecosystem at IJR was suggested to have been acidified and N-saturated in the mid-1990s, followed by a recovery since the 2000s (Nakahara et al., 2010; Sase et al., 2019). Consistent with this recovery, DIN concentrations in stream water have continuously decreased since 2007 (Fig. 5.6.2). Nevertheless, DIN equivalent to nearly 70% of the atmospheric N input is still exported via stream water. This indicates that N saturation has not been fully alleviated, and continued monitoring is necessary to adequately assess the ecosystem's recovery process.

4) LMW

At La Mesa Watershed, atmospheric inputs of S generally exceeded outputs via stream water during the 2019–2023 observation period, indicating that a portion of deposited S was retained within the catchment. However, SO_4^{2-} concentrations in stream water were generally higher than those in rainwater in most years, suggesting that stream-water SO_4^{2-} was not controlled solely by current atmospheric deposition. Internal catchment processes, including soil and groundwater interactions, hydrologic flushing, delayed release of stored S, or possible geologic S sources, may have contributed to the observed stream-water sulfate levels.

In contrast, DIN output via stream water was consistently lower than atmospheric DIN input. This indicates that a substantial fraction of deposited inorganic N was retained, transformed, or utilized within the forest ecosystem. In forest catchments, N is commonly assimilated by vegetation and soil microorganisms, and only limited amounts are leached to stream water when ecosystem N demand remains high. The relatively low DIN export at La Mesa Watershed therefore suggests that the catchment continues to function as an effective N sink.

The marked increase in atmospheric DIN input in 2023 was not accompanied by a proportional increase in stream-water DIN output. This further indicates that the watershed retained much of the additional N input during the observation period. Nevertheless, continued N deposition may gradually reduce the N retention capacity of the ecosystem and increase the risk of N saturation and downstream NO_3^- export. Continued monitoring of DIN input-output balances, including NH_3 and NH_4^+ deposition, is therefore necessary to assess the long-term response of the La Mesa Watershed forest ecosystem to atmospheric N loading.

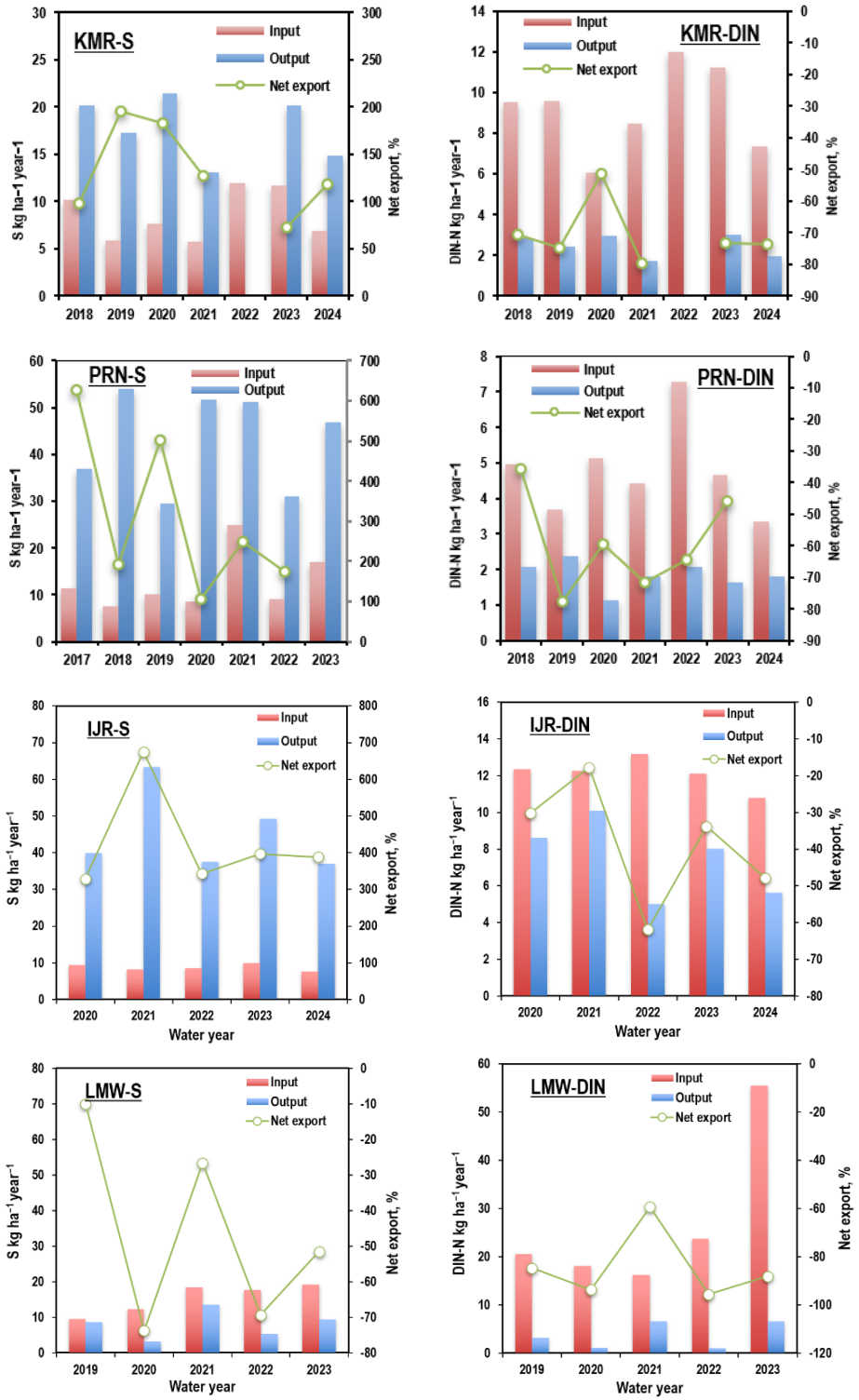

Fig. 5.6.3 Input-output budget on sulfur (S) and dissolved inorganic nitrogen (DIN) at the IJR for the period from 2020 to 2024 at KMR, PRN, IJR, and LMW. Input, atmospheric total deposition; output, stream water flux. In KMR, the output for 2022 is not calculated.

5.6.3 Status of nitrogen leaching from forest ecosystems

As discussed above, excessive atmospheric N inputs may disturb biogeochemical cycles and accelerate N leaching to streams. The relationship between atmospheric N inputs and the leaching of DIN into stream water is shown in Fig. 5.6.4. To account for time lags associated with biogeochemical and hydrological processes within ecosystems, three-year moving averages of atmospheric inputs and stream-water concentrations were used for comparison. Data from the former

EANET project site, the Kajikawa catchment site (KJK) (Sase et al. 2021), are also shown for reference. Previous studies have discussed threshold values of atmospheric N deposition for N leaching from forest ecosystems; empirical critical loads in boreal and temperate forests in Europe range 7 to 15 kg N ha^{-1} $year^{-1}$ (Xie et al., 2018), which is also shown in the figure.

No clear relationship between atmospheric N deposition and N leaching was observed at these sites, except for IJR. At IJR, stream-water NO_3^- concentrations clearly decreased in response to the decline in atmospheric N deposition. High DIN concentrations tended to occur in forested catchments where N deposition was comparable to or exceeded the empirical critical load for N.

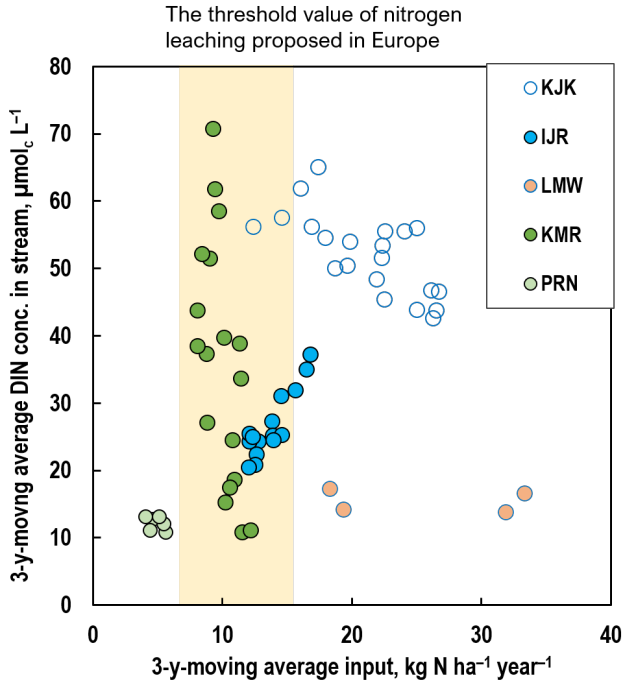

Fig. 5.6.4 Relationship between atmospheric nitrogen (N) inputs and leaching of dissolved inorganic nitrogen (DIN) to stream water at EANET catchment sites. Three-year moving averages of total N deposition (wet and dry) and stream-water DIN concentrations are shown. The yellow band indicates the range of threshold value for leaching proposed in Europe (7 – 15 kg N ha^{-1} $year^{-1}$). KJK, Kajikawa catchment site, surveyed by the EANET project until 2025 (modified from Sase et al. 2021).

5.6.4 Summary

Catchment-scale analyses of four forested catchments in three countries revealed that stream water chemistry did not always respond immediately to changes in atmospheric deposition. At IJR, which had previously been acidified and N-saturated, stream water SO_4^{2-} and DIN concentrations, mostly NO_3^-, decreased in association with declining atmospheric deposition, suggesting ongoing recovery processes. However, at the other sites, no clear relationship with atmospheric deposition was observed during the observation period. Other factors, such as meteorological and hydrological conditions, appeared to influence S and N leaching processes. At LMW, atmospheric deposition is still increasing; therefore, possible delayed responses of the forest ecosystem should be carefully monitored. For S, multiple sources, including atmospheric deposition, geological S, and previously accumulated S, should be considered. Atmospheric N deposition does not necessarily control N leaching to stream water. High DIN concentrations tended to occur in forested catchments where N deposition was comparable to or exceeded the empirical critical load for N; however, LMW showed relatively low DIN concentrations despite elevated N deposition. The DIN input–output budgets suggest that the surveyed forest catchments are still functioning as N sinks. However, the relatively

high output-to-input ratio observed at IJR indicates that N retention may remain incomplete. Continued monitoring of atmospheric N deposition and DIN leaching is therefore necessary.

5.7 Conclusions

EANET ecological monitoring over more than two decades has accumulated substantial datasets on soil, forest vegetation, and inland water to assess the impacts of atmospheric deposition on ecosystems. In addition, catchment-scale analyses have helped clarify the interrelationships among atmospheric deposition, soil, forest vegetation, and stream water.

Diverse soil chemical properties across EANET sites are primarily controlled by soil formation processes, forest composition, and climatic conditions. At several sites in China and Japan, soil pH increased as nss-SO_4^{2-} wet deposition decreased. However, temporal changes in soil pH did not necessarily follow trends in atmospheric deposition of acidic substances, suggesting complex soil responses.

Forest growth monitored continuously in China and Japan showed no significant increase corresponding to the decrease in nss-SO_4^{2-} wet deposition since 2007. Most observed changes can be attributed to human disturbance, climate fluctuations, or increased competition among individuals as forest stands age.

Inland water chemistry showed no clear regional evidence of widespread acidification across the EANET monitoring sites. Long-term trends varied among sites; however, decreases in SO_4^{2-} concentrations were observed more frequently than increases, suggesting a partial response to reductions in sulfur deposition. The correspondence between atmospheric deposition and inland water chemistry was clearer for sulfur-related parameters than for nitrogen-related parameters.

Catchment-scale analyses revealed that stream water chemistry did not always respond immediately or directly to changes in atmospheric deposition. Decreases in stream water SO_4^{2-} and NO_3^- were observed where atmospheric deposition had declined, suggesting ongoing recovery from acidification and N saturation. However, such relationships were not consistent across all catchments. The surveyed forest catchments generally still function as N sinks, although incomplete N retention may occur under conditions of relatively high DIN export.

Overall, ecosystem responses were not always consistent with changes in atmospheric deposition, indicating strong influences of meteorological, hydrological, geological, and internal biogeochemical processes at individual monitoring sites. At the same time, relationships between atmospheric deposition and ecosystem responses were observed at several sites, and atmospheric deposition is still increasing at some sites. It has become clear that there is considerable variation in the responses of vegetation, water bodies and catchment areas across different regions to changes in atmospheric deposition, and that it is difficult to assess these impacts uniformly based solely on the deposition levels of N and S compounds. In particular, CO_2 concentrations and temperatures continue to rise year on year, whilst precipitation levels and patterns are also changing. These environmental factors have the potential to exert a significant influence, both directly and indirectly, on ecosystem responses. It will be necessary to situate ecosystem monitoring within the context of such environmental changes. Continued monitoring of atmospheric deposition and ecosystem responses is therefore necessary to detect delayed recovery, acidification, and possible changes in N retention.

5.8 References

Baba, M., Okazaki, M. 1998. Acidification in nitrogen-saturated forested catchment. Soil Science and Plant Nutrition, 44, 513–525.

Berg, B., McClaugherty, C. 2008. Plant Litter: Decomposition, Humus Formation, Carbon Sequestration, third ed. Springer.

Breemen, N. Van, Driscoll, C. T., Mulder, J. 1984. Acidic deposition and internal proton sources in acidification of soils and waters. Nature, 307(5952), 599–604.

Duan, L., Yu, Q., Zhang, Q., Wang, Z., Pan, Y., Larssen, T., Tang, J., Mulder, J. 2016. Acid deposition in Asia: Emissions, deposition, and ecosystem effects. Atmospheric Environment, 146, 55–69.

EANET. 2000. Technical documents for soil and vegetation monitoring in East Asia.

EANET 2010a. Technical Manual for Inland Aquatic Environment Monitoring in East Asia -2010, Network Center for Acid Deposition Monitoring Network in East Asia (EANET), Asia Center for Air Pollution Research (ACAP), Niigata, Japan.

EANET 2010b. Guideline for Catchment-scale Monitoring in East Asia, Network Center for Acid Deposition Monitoring Network in East Asia (EANET), Asia Center for Air Pollution Research (ACAP), Niigata, Japan.

IUSS Working Group WRB. 2015. World Reference Base for Soil Resources 2014, update 2015. International soil classification system for naming soils and creating legends for soil maps. World Soil Resources Reports No. 106. FAO, Rome.

Larssen, T., Carmichael, G. R. 2000. Acid rain and acidification in China: the importance of base cation deposition. Environmental Pollution, 110(1), 89–102.

Oyanagi, N., Chihara, M., Toda, H., Haibara, K. 2002. Characteristics of carbon and nitrogen mineralization of forest soils in different slopes and vegetation. Journal of Japanese Forest Society, 84, 111-119 (in Japanese with English summary).

Takahashi, T., Toda, H., Haibara, K. 1999. Changes in soil chemical and physical characteristics in Japanese cypress (*Chamaecyparis obtusa* Endl.) stands by mixture of deciduous broad-leaved trees in the northern Kanto region of Japan. Journal of Forest Research, 4, 223-228.

EANET. 2000. Technical documents for soil and vegetation monitoring in East Asia.

Forzieri, G., Girardello, M., Ceccherini, G. et al. 2021. Emergent vulnerability to climate-driven disturbances in European forests. Nature Communications, 12, 1081. https://doi.org/10.1038/s41467-021-21399-7

Hisano, M., Chen, H.Y.H., Searle, E.B., Reich, P.B. 2020. Species-rich boreal forests grew more and suffered less mortality than species-poor forests under the environmental change of the past half-century. Ecology Letters, 22, 999-1008. https://doi.org/10.1111/ele.13259

Ishida, M., Nakajima, H., Kume, A. 2026. The Impacts of Climate Warming on the Forest Vegetation Zone on Mt. Tateyama, Japan: Findings From Long-Term Forest Monitoring (1998–2024) and Meteorological Observation Data. Journal of Vegetation Science, in press

Kume, A., Fujimoto, M., Mizoue, N., Honoki, H., Nakajima, H., Ishida, M. 2020. Impact of reduced ozone concentration on the mountain forests of Mt. Tateyama, Japan. Environmental Pollution, 267, 115407. https://doi.org/10.1016/j.envpol.2020.115407.

Okamoto, S., Tanimoto, H., Hirota, N., Ikeda, K., Akimoto, H., 2018. Decadal shifts in wind patterns reduced continental outflow and suppressed ozone trend in the 2010s in the lower troposphere over Japan. Journal of Geophysical Research: Atmospheres, 123. https://doi.org/10.1029/2018JD029266

Driscoll, C. T. and van Dreason, R. 1993. Seasonal and long-term temporal patterns in the chemistry of Adirondack lakes. Water Air Soil Pollut. 67: 319-344.

Driscoll, C. T., Lawrence, G. B., Bulger, A. J., Butler, T. J., Cronan, C. S., Eager, C., Lambert, K. F., Likens, G. E., Stoddard, J. L., and Weathers, K. C. 2001. Acidic Deposition in the Northeastern United States: Sources and Inputs, Ecosystem Effects, and Management Strategies. BioScience, 51: 180-198.

Duan, L., Yu, Q., Zhang, Q., Wang, Z., Pan, Y., Larssen, T., Tang, J. and Mulder, J. 2016. Acid deposition in Asia: Emissions, deposition, and ecosystem effects. Atmos. Environ. 146: 55–69.

Ohte, N. 2025. Ecosystem responses and behaviors under changing pressure of air pollutants: Special article collection from the 10th International Conference on Acid Deposition “ACID RAIN 2020”. Ecological Research 40: 245–248.

Sase, H., Takahashi, M., Matsuda, K., Sato, K., Tanikawa, T., Yamashita, N., Ohizumi, T., Ishida, T., Kamisako, M., Kobayashi, R., Uchiyama, S., Saito, T., Morohashi, M., Fukuhara, H., Kaneko, S., Inoue, T., Yamada, T., Takenaka, C., Tayasu, I., Nakano, T., Hakamata, T., & Ohta, S. (2019). Response of river water chemistry to changing atmospheric environment and sulfur dynamics in a forested catchment in central Japan. Biogeochemistry, 142, 357–374.

Aber, J.D., Goodale, C.L., Ollinger, S.V., Smith, M.-L., Magill, A.H., Martin, M.E., Hallett, R.A., Stoddard, J.L. 2003. Is nitrogen deposition altering the nitrogen status of northeastern forests? BioScience 53, 375–389. https://doi.org/10.1641/0006-3568(2003)053[0375:INDATN]2.0.CO;2

Aber, J. D., McDowell, W., Nadelhoffer, K., Magill, A., Berntson, G., Kamakea, M., McNulty, S., Currie, W., Rustad, L., Fernandez, I. 1998. Nitrogen saturation in temperate forest ecosystems: hypotheses revisited. BioScience 48, 921–934.

EANET 2010. Technical Manual for Dry Deposition Flux Estimation in East Asia–2010, Network Center for Acid Deposition Monitoring Network in East Asia (EANET), Asia Center for Air Pollution Research (ACAP), Niigata, Japan.

Nakahara, O., Takahashi, M., Sase, H., Yamada, T., Matsuda, K., Ohizumi, T., Fukuhara, H., Inoue, T., Takahashi, A., Kobayashi, H., Hatano, R., Hakamata, T. 2010. Soil and stream water acidification in a forested catchment in central Japan. Biogeochemistry 97, 141-158. https://doi.org/10.1007/s10533-009-9362-4

Saito, T., Nakata, M., Yamashita, N., Inomata, Y., Uchiyama, S., Ohizumi, T., Sase, H. 2023. Vertical changes in sulfur isotopic ratio of water flowing through a forested catchment along the coast of the Sea of Japan in central Japan–a buffer against seasonal transboundary air pollution. Journal of Forest Research 28:4, 240-250. https://doi.org/10.1080/13416979.2023.2198113

Sase, H., Saito, T., Takahashi, M., Morohashi, M., Yamashita, N., Inomata, Y., Ohizumi, T., Nakata, M. 2021. Transboundary air pollution reduction rapidly reflected in stream water chemistry in forested catchment on the Sea of Japan coast in central Japan. Atmospheric Environment 248, 118223. https://doi.org/10.1016/j.atmosenv.2021.118223.

Sase, H., Takahashi, M., Matsuda, K., Sato, K., Tanikawa, T., Yamashita, N., Ohizumi, T., Ishida, T., Kamisako, M., Kobayashi, R., Uchiyama, S., Saito, T., Morohashi, M., Fukuhara, H., Kaneko, S., Inoue, T., Yamada, T., Takenaka, C., Tayasu, I., Nakano, T., Hakamata, T., Ohta, S. 2019. Response of river water chemistry to changing atmospheric environment and sulfur dynamics in a forested catchment in central Japan. Biogeochemistry 142, 357-374. https://doi.org/10.1007/s10533-019-00540-1

Stoddard, J. L. 1994. Long-term changes in watershed retention of nitrogen. In: L. A. Baker, ed. Environmental chemistry of lakes and reservoirs. Advances in Chemistry Series. Volume 237 pp. 223–284.

Xie, D., Duan, L., Du, E., de Vries, W. 2024. Chapter 14 - Indicators and thresholds for nitrogen saturation in forest ecosystems. In: Editor(s): Enzai Du, Wim de Vries, Atmospheric Nitrogen Deposition to Global Forests, Academic Press, pp. 249-261,

Zhigacheva, E. S., Sase, H., Nakata, M., Ohizumi, T., Gromov, S. A., & Takahashi, M. 2022. Stream water acidification in the Far East of Russia under changing atmospheric deposition and precipitation patterns. Limnology 23, 415–428. https://doi.org/10.1007/s10201-022-00696-0